Noncoaxial K-feldspar and AMS subfabrics in the Land's End granite, Cornwall: Evidence of magmatic fabric decoupling during late deformation and matrix crystallization

Zuzana Kratinová,[1,2] Josef Ježek,[3] Karel Schulmann,[4] František Hrouda,[5,6] Robin K. Shail,[7] and Ondrej Lexa[6]

Received 23 June 2009; revised 26 March 2010; accepted 11 May 2010; published 28 September 2010.

[1] A comparative study of the anisotropy of magnetic susceptibility (AMS) and K-feldspar phenocryst fabrics in the Land's End granite demonstrates that the AMS fabric predominantly reflects late magmatic deformation. Tensor analysis of the K-feldspar fabric shows a complex pattern, characterized by meter-scale variations in orientation, symmetry, and intensity, mainly related to heterogeneous flow of the phenocryst-rich magma during emplacement. In contrast, the AMS fabric is predominantly homogenous, subhorizontal, and oblate, and is stable at the pluton scale. Quantitative microstructural analysis suggests that the AMS fabric is controlled by deformation of the partially crystallized matrix, resulting from the combined effects of late internal adjustment within the pluton and regional deformation. A general model of fabric development associated with a vertical pure-shear overprint on a variable vertical fabric is evaluated by numerical modeling. The study demonstrates how the memory of different fabric elements may be dependent upon their grain size, crystallization sequence, and recorded previous strain.

Citation: Kratinová, Z., J. Ježek, K. Schulmann, F. Hrouda, R. K. Shail, and O. Lexa (2010), Noncoaxial K-feldspar and AMS subfabrics in the Land's End granite, Cornwall: Evidence of magmatic fabric decoupling during late deformation and matrix crystallization, *J. Geophys. Res.*, *115*, B09104, doi:10.1029/2009JB006714.

1. Introduction

[2] The anisotropy of magnetic susceptibility (AMS) is an efficient petrophysical method to investigate the preferred orientation of magnetic minerals in a rock [*Tarling and Hrouda*, 1993; *Borradaile and Henry*, 1997; *Borradaile and Jackson*, 2004]. AMS has been extensively used for characterizing the internal fabrics and emplacement history of granites [e.g., *Bouchez*, 1997]. Techniques have been developed that integrate the regional mapping of AMS fabric characteristics (orientation of foliation and lineation, fabric symmetry, degree of anisotropy) with detailed microstructural evaluation [e.g., *Bouchez*, 2000; *Gleizes et al.*, 2006]. In combination with strain analysis of the host rocks, AMS studies have provided structural, microstructural, and fabric data consistent with important coupling between magma emplacement, cooling, and large-scale tectonics [e.g., *Aurójac et al.*, 2004; *Žák et al.*, 2005; *Kratinová et al.*, 2007]. However, such interpretations are usually based on an assumption that the AMS fabric corresponds to a magmatic fabric generated during the emplacement process [*Paterson et al.*, 1998]. Attempts have been made to correlate the AMS fabric with the orientation of magnetic carriers at the microscopic scale [*Launeau and Cruden*, 1998] as well as the relationship between AMS and the orientation tensor [*Hrouda and Schulmann*, 1990; *Ježek and Hrouda*, 2000] and the influence of magnetic carrier shape [*Hrouda and Ježek*, 1999].

[3] However, magmatic fabrics are not only formed by ferro or paramagnetic carriers, but also by diamagnetic rock-forming minerals and objects like mafic enclaves, schlieren, and boundaries between different magmatic units [*Paterson et al.*, 1998]. Other detailed field-based structural studies have indicated that plutonic fabrics result from internal magmatic processes such as magma pulses and surges driven by contrasts in gravitational potential within magma chambers [*Miller and Paterson*, 1999, 2001]. These studies have highlighted the complexity of magma chamber construction, whereby material transfer processes may result in the development of multiple superposed magmatic fabrics [e.g., *Žák et al.*, 2005, 2008]. It has also been recently demonstrated that, in some cases, late and often weak fabrics crosscut boundaries between magmatic units and result from late deformation overprints that are not causally

[1]Institute of Geophysics, Czech Academy of Sciences, Prague, Czech Republic.
[2]University of Lisbon and IDL, Lisbon, Portugal.
[3]Institute of Applied Mathematics and Computer Sciences, Charles University, Faculty of Science, Prague, Czech Republic.
[4]Centre de Géochimie de la Surface, EOST, UMR 7516, Université Louis Pasteur, Strasbourg cedex, France.
[5]Agico Inc., Brno, Czech Republic.
[6]Institute of Petrology and Structural Geology, Charles University, Prague, Czech Republic.
[7]Camborne School of Mines, College of Engineering, Mathematics and Physical Sciences, University of Exeter, Cornwall Campus, Penryn, United Kingdom.

0148-0227/10/2009JB006714

related to magma emplacement processes [*Žák et al.*, 2007, 2008].

[4] Meaningful integration of petrophysical and field-based structural data requires an understanding of the relationship between the AMS fabric and the magmatic fabric determined in the field. Little work has previously been focused on comparative studies of AMS fabrics and nonmagnetic fabric elements [e.g., *Borradaile and Kehlenbeck*, 1996; *Borradaile and Gauthier*, 2003]. *Launeau and Robin* [1996] developed an image analysis method based on measuring fabric orientations from mutually orthogonal sections. The orientation of these sections is usually chosen with respect to the AMS ellipsoid, which makes this method particularly suitable to evaluate the correlation between rock and AMS fabrics. However, in the case of nonmagnetic minerals, this correlation can be biased by the choice of the reference planes. An alternative fabric analysis method using optical reflection goniometry has been developed by *Venera et al.* [1996] in order to measure the orientation of large feldspar crystals that form an ubiquitous element of the magmatic fabric. This method is the only one that allows the orientation tensor of large nonmagnetic minerals to be defined so that it can be correlated with the AMS tensor.

[5] In this work we demonstrate a methodology for the quantitative evaluation of the relationship between the AMS fabric and the magmatic fabric in a paramagnetic granite. We have compared the AMS fabric (essentially carried by biotite) and the magmatic fabric defined by large feldspar phenocrysts within the Land's End granite in Cornwall (southwest England). We evaluate these two fabric types with respect to different scales of observation, localization of the samples, fabric intensity, and dominant regional tectonic trends. We then propose a model of differential fabric memory between the large feldspar crystals and matrix biotite that is supported by microstructural observations and numerical modeling of fabric development. Our study demonstrates that the AMS fabric has a high sensitivity to late deformation overprinting and the crystallization of interstitial melt, and is essentially decoupled from the feldspar fabric that largely records the earlier stages of magma emplacement. Magmatic state AMS fabrics elsewhere may have been influenced by similar processes but the combined use of the AMS and other fabric analysis methods has the potential to provide complete information about magma emplacement and transfer processes at local and crustal scales.

2. Geological Setting

[6] The Land's End granite is the youngest of the five mainland plutons of the early Permian Cornubian batholith (Figure 1a). It is a representative example of a peraluminous, S-type anatectic granite [*Chappell and Hine*, 2006] and has a predominantly crustal origin [*Müller et al.*, 2006]. The Cornubian batholith is located within the lower plate of the Variscan Rhenohercynian/Rheic suture [*Shail and Leveridge*, 2009]. During the latest Carboniferous, Variscan convergence across much of northwest Europe was succeeded by a dextral transtensional regime, controlled by major NW–SE faults [e.g., *Arthaud and Matte*, 1977; *Ziegler and Dèzes*, 2006]. In southwest England this regime brought about the extensional reactivation of the Rhenohercynian/Rheic suture, together with movements on other Variscan thrusts and NW–SE transfer faults, exhumation of the lower (northern) plate, and the generation and emplacement of the Cornubian batholith [*Shail and Leveridge*, 2009].

[7] The Land's End pluton primarily comprises coarse-grained to medium-grained porphyritic biotite granite and fine-grained biotite granite [*Booth and Exley*, 1987; *Müller et al.*, 2006]. Mingling and mixing between these magmas resulted in chemical and textural inhomogeneity of the pluton [*Salmon*, 1994].

[8] Emplacement of the batholith, constrained by U-Pb dating of magmatic monazite and xenotime, spans some 20 Ma during the Early Permian, ranging from 293 ± 1.3 Ma for the Carnmenellis granite to 274.5 ± 1.4 Ma for the Land's End granite [*Chen et al.*, 1993; *Chesley et al.*, 1993]. Individual plutons are composite and, at the current exposure level, appear to have been constructed by magma batches emplaced over ~3–5 Ma [*Chen et al.*, 1993; *Chesley et al.*, 1993]. In the Land's End pluton, the mineralogically and texturally similar megacrystic coarse-grained biotite granites forming the NE and SW lobes represent separate intrusive centers [*Clark et al.*, 1994]. In the NE, the fine-grained granite at Castle-an-Dinas (276.7 ± 0.4 Ma) is indistinguishable, within error, from nearby coarse-grained biotite granite (277.1 ± 0.4 Ma) at Crippleseae, and in the SW, the fine-grained granite at Polgigga (274.4 ± 0.4 Ma) is indistinguishable from the coarse-grained biotite granite at Lamorna Cove (274.7 ± 0.4 Ma) [*Clark et al.*, 1994].

2.1. Host Rock Deformation

[9] The Land's End granite intrudes intercalated metasedimentary and metavolcanic rocks of the upper Devonian Mylor Slate Formation i.e., [*Goode and Taylor*, 1988; Figure 1b]. In common with other Devonian successions in SW England, the host rocks underwent two episodes ($D_1 + D_2$) of Variscan NNW–SSE convergence-related deformation during the Carboniferous [*Rattey and Sanderson*, 1984; *Shail and Leveridge*, 2009]. Peak low-grade regional metamorphism occurred during D_1 [*Warr et al.*, 1991]. Toward the end of the Carboniferous, there was a change to a NNW–SSE extensional tectonic regime [*Dearman*, 1971; *Hawkes*, 1981; *Shail and Wilkinson*, 1994; *Shail and Leveridge*, 2009]. A subhorizontal to gently NNW-dipping foliation (S_3), and asymmetrical folds (F_3) that verge predominantly to the SSE (Figure 1b) were developed throughout the Mylor slate formation in response to thrust fault reactivation [*Alexander and Shail*, 1995, 1996; *Hughes et al.*, 2009]. The ductile D_3 fabric recorded in the host rocks largely predates granite emplacement but is overprinted, in both the host rocks and all plutons, by ENE–WSW striking extensional faults and tensile fractures, and NNW–SSE striking transfer faults, and implies that the regional NNW–SSE extensional regime persisted throughout the 20 Ma of batholith emplacement [*Shail and Wilkinson*, 1994; *Shail and Alexander*, 1997; *Shail and Leveridge*, 2009]. The host rocks have a low pressure amphibolite facies contact metamorphic overprint in the vicinity of the granite [*Goode and Taylor*, 1988] and abundant stoped blocks provide additional constraints on fabric formation.

2.2. Emplacement Models

[10] Emplacement models for the Cornubian batholith are poorly developed. *Ghosh* [1934] undertook pioneering

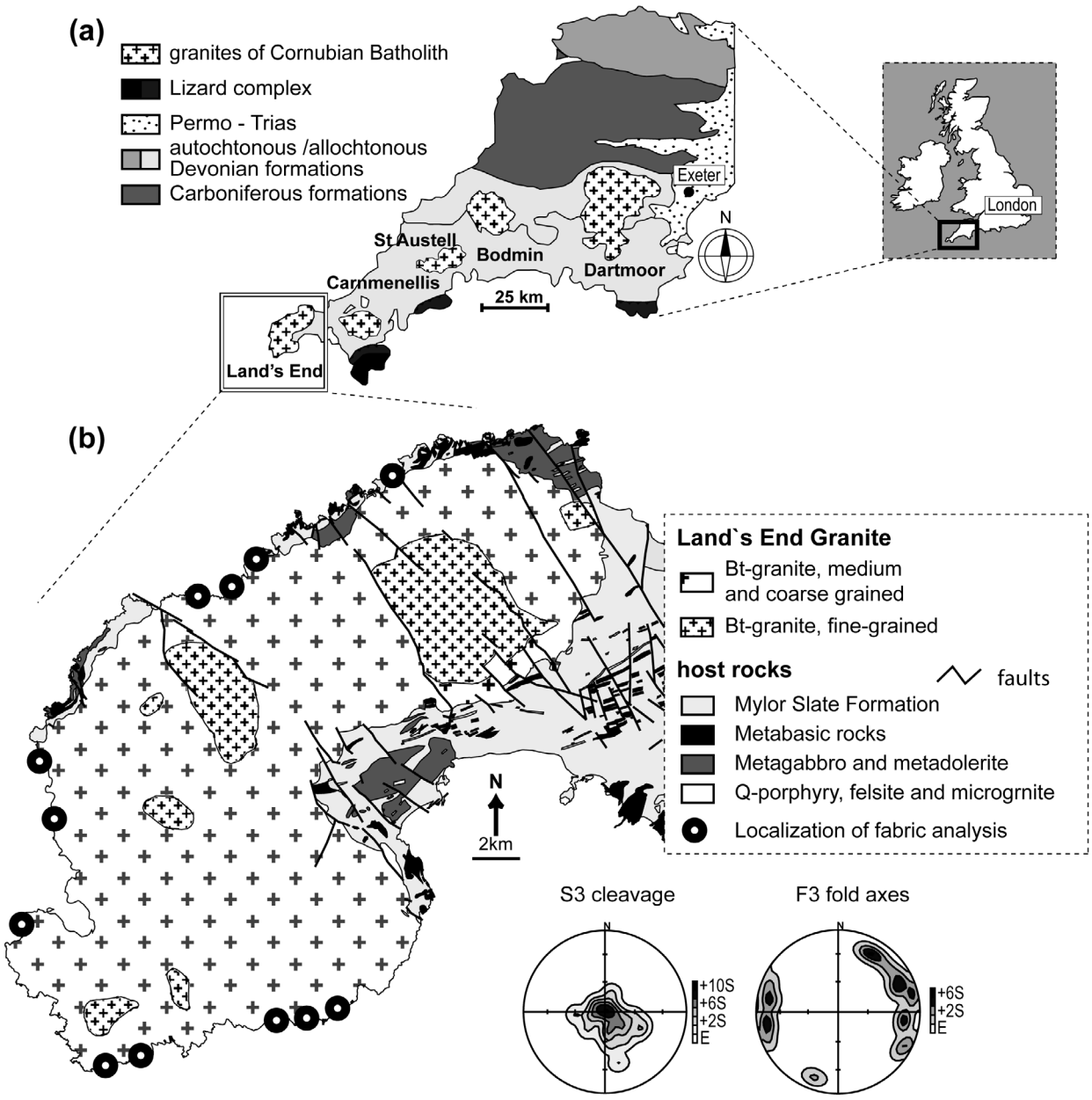

Figure 1. Geology of the Land's End granite and its host rock. (a) Simplified geological map of the SW England with indicated granite plutons of the Cornubian batholith (after British Geological Survey map, 1984). (b) Geological map of the Land's End granite and its host rocks. Profiles selected for detailed fabric analysis are indicated by open circles. Contoured diagrams (equal-area lower hemisphere projection) of poles to S_3 foliation planes and axes of F_3 folds.

fabric studies on the adjacent Carnmenellis granite and concluded that the granite magma was emplaced from the south, which locally gave rise to steep foliations, but more generally developed a gently inclined foliation during movement to the NNW. Few detailed fabric studies have been undertaken until recently, in part reflecting the locally prevalent metasomatic interpretation of K feldspars during the 1960s–1980s [e.g., *Stone and Austin*, 1961] and there was a presumption of a diapiric emplacement mechanism [e.g., *Rattey and Sanderson*, 1984; *Booth and Exley*, 1987]. The AMS fabrics in the Carnmenellis granite were described by *Minsta Mi Nguema et al.* [2002]; their results largely supported the work of *Ghosh* [1934] and confirmed the dominance of a NW–SE magma stretch during emplacement. Broadly similar conclusions were obtained from an analysis of AMS fabrics in the Bodmin Moor granite [*Bouchez et al.*, 2006]; fabrics, including a weak solid-state component, were generally more intense toward the pluton margins and a NNW–SSE AMS lineation was interpreted as the direction of magma stretch. D_3 and earlier structures were tilted away from the plutons during emplacement, particularly along their northern margins [e.g., *Rattey and Sanderson*, 1984; *Hughes et al.*, 2009]. Bedding, metabasic rocks, and the trace of S_1 cleavage are all deflected around the northern

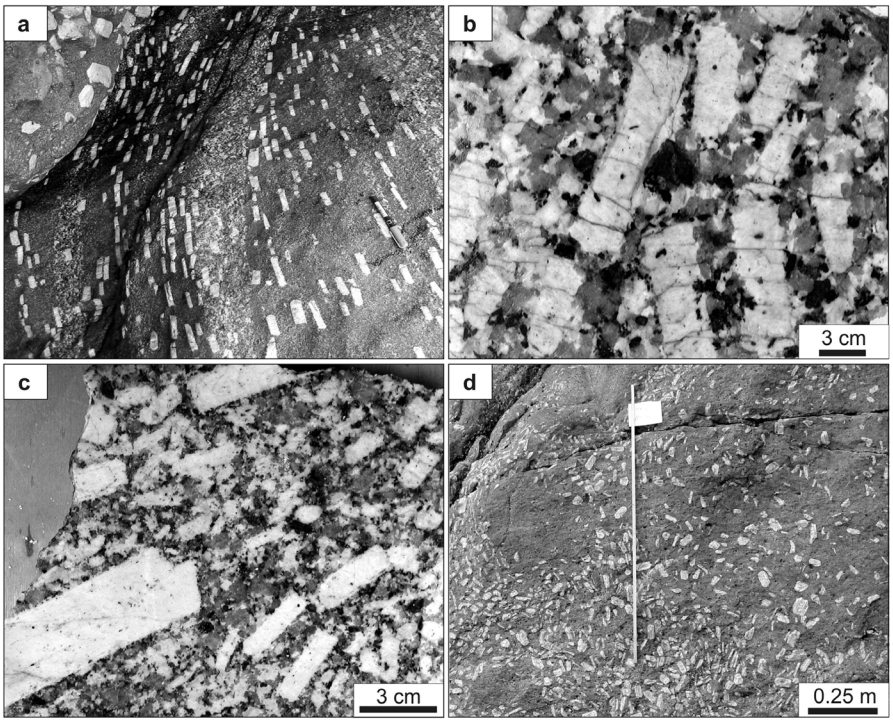

Figure 2. Field photographs of main textural types of the Land's End granite. (a) Macroscopic magmatic foliation defined by the preferred orientation of large K feldspars. (b) Main textural type marked by equidimensional K feldspars. (c) Bimodal grain size distribution of K-feldspar crystals. (d) Weak K-feldspar phenocrysts preferred orientation pattern.

half of the Carnmenellis granite [*Ghosh*, 1934; *Leveridge et al.*, 1990]. These features plus the distribution of fault zones were interpreted by *Ghosh* [1934] as evidence of forceful emplacement; a theme supported by the magnetic fabric studies of *Rathore* [1980] and expanded by *Taylor* [2007], who suggested they defined marginal synclines compatible with roof uplift during emplacement. Similar deflections of the regional strike of bedding and S_1 cleavage occur around the northern margins of the Bodmin Moor, Dartmoor, and to a lesser extent, the St. Austell granites. Near-surface pluton geometry is strongly influenced by the interaction between NW–SE and ENE–WSW moderately to steeply dipping faults and it has been suggested that these faults may act coevally to generate rhomboidal pull-aparts [*Shail and Wilkinson*, 1994].

3. Magmatic Fabrics and Microstructures

[11] The main textural variety within the Land's End granite is a medium-grained to coarse-grained porphyritic biotite granite with a variable modal content and size of feldspar phenocrysts [*Dangerfield and Hawkes*, 1978]. Euhedral K-feldspar megacrysts 2–4 cm in length exclusively define the macroscopic magmatic fabrics (Figure 2a). The main texture is characterized by equidimensional feldspar phenocrysts (Figure 2b). Locally, a bimodal size distribution is developed with large phenocrysts up to 20 cm associated with small feldspars around 2 cm that show the same preferred orientation (Figure 2c). Recent geochemical investigations indicate that the large feldspar phenocrysts represent xenocrysts that crystallized earlier at higher temperatures in a moderately evolved magma [*Müller et al.*, 2006].

3.1. Magmatic fabrics

[12] A strong magmatic fabric is predominantly defined by the alignment of feldspar phenocrysts in the absence of solid-state deformation. The magmatic foliation exhibits a complex orientation pattern; two main alignment directions have been recognized and are associated with meter-scale local variations. A relatively scattered distribution of foliation shows maximum concentration moderately dipping to NE and E that locally alternates with a NNW–SSE trending

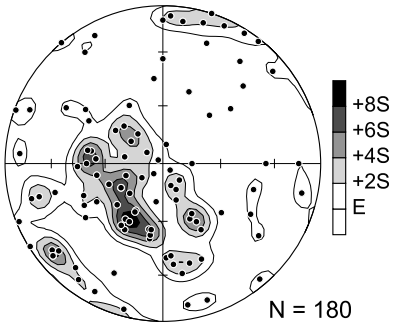

Figure 3. The contoured stereogram (equal-area lower hemisphere projection) of poles to field magmatic foliation planes defined by the preferred orientation of large K feldspars. The stereonet comprises the general feldspar foliation in the homogeneous Land's End granite and also the feldspar fabrics close to stoped blocks.

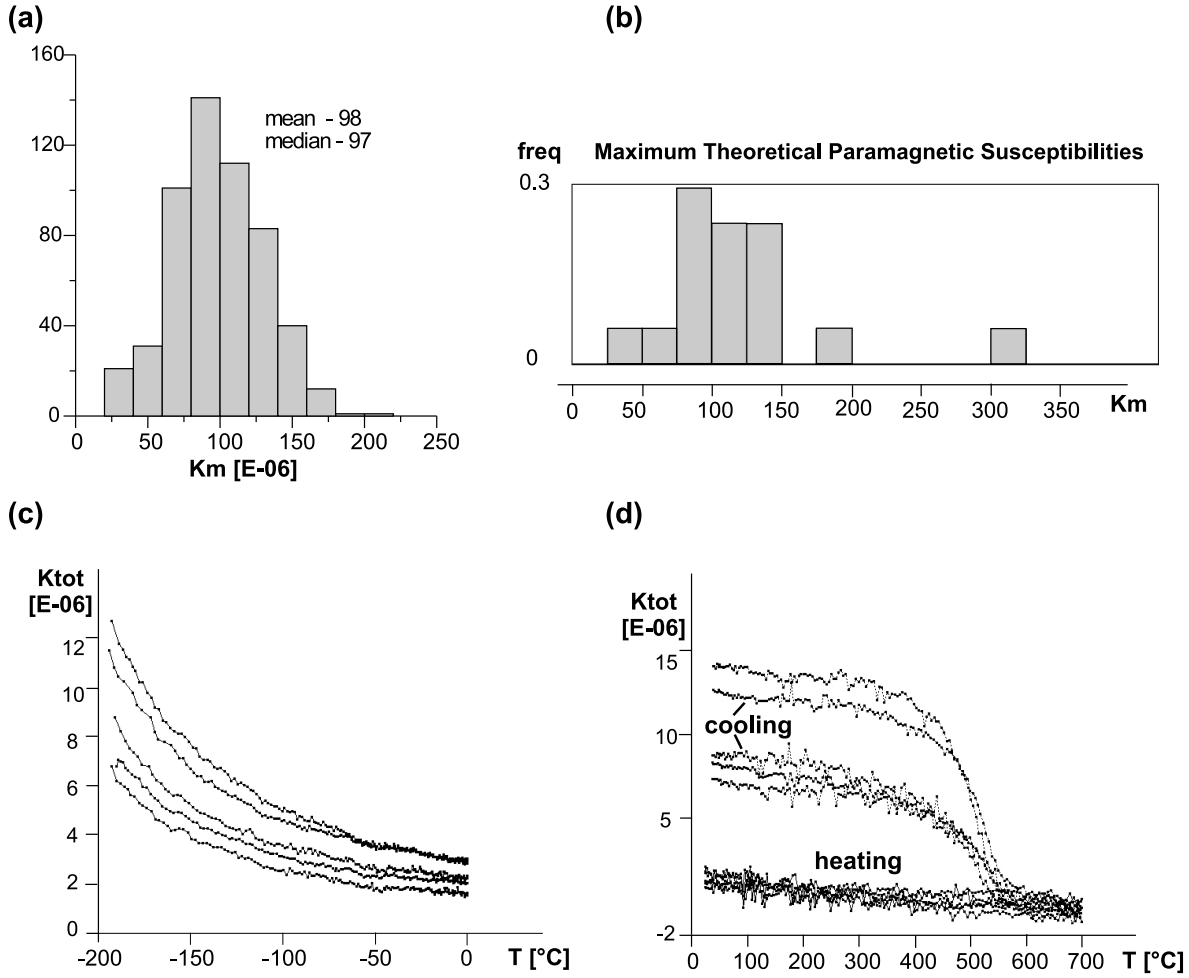

Figure 4. Magnetic mineralogy diagrams. (a) Histogram of mean magnetic susceptibility Km. (b) The maximum theoretical paramagnetic susceptibility (MTPS) calculated from chemical analyses [*Chappell and Hine*, 2006; *Müller et al.*, 2006]. (c) Diagram of bulk susceptibility versus temperature for low temperatures. (d) Diagram of bulk susceptibility versus temperature for high temperatures.

vertical foliation (Figure 3). Magmatic lineations were generally difficult to identify but, where observed, are NNW–SSE subhorizontbal to locally vertical. The intensive fabrics alternate with domains of weak fabric or even unaligned phenocrysts with a rather chaotic fabric pattern (Figure 2d). In addition, magmatic foliations tend toward parallelism with the margins of stoped blocks and roof of the pluton over a distance of one to several meters and exhibit meter-scale variations with respect to stoped blocks [*Kratinová et al.*, 2003].

3.2. Microstructure

[13] The microstructures of the Land's End granite are generally magmatic without any significant solid-state overprints [*Paterson et al.*, 1989]. The groundmass of the coarse-grained to medium-grained granite is formed by large subhedral feldspars embedded in a matrix of plagioclase, biotite, interstitial anhedral quartz, K feldspar, and muscovite. Tourmaline is also locally developed as an accessory mineral. The generally microperthitic K feldspars show rapakivi textures and often enclose plagioclase, quartz, and biotite inclusions. These are usually concentrically distributed along irregular internal boundaries. Subhedral to anhedral tabular plagioclase phenocrysts up to 4 cm in length display typical magmatic growth zoning patterns and sieve textures are common. The frequent compositional zoning within the plagioclase indicates disequilibrium during magma crystallization. The crystallization of K feldspar is assumed to be predominantly a temperature-sensitive process having nucleation temperature not far above solidus [*Flood and Vernon*, 1988], which suggests that the pluton underwent a relatively complex cooling history related to local reheating. In general, many features such as disrupted zones and corroded crystal shapes suggest the importance of dissolution and resorption indicating that the final texture results from a chemically open system. In addition, the trace element patterns of the K feldspars, including Ba profiles, point to crystallization within different magma batches, possibly at different times [*Müller et al.*, 2006].

4. Anisotropy of Magnetic Susceptibility: Biotite Preferred Orientation

[14] The oriented samples were drilled with a petrol-driven portable drilling machine and were locally supple-

mented by larger orientated field specimens that were examined in the laboratory. The AMS was measured on 1080 samples; for the detailed fabric comparative study we have used selected 12 cross sections in Figure 1b containing 420 samples with an average of 12 samples per station. The low field AMS was measured with a KLY-3S Kappabridge in Agico [*Jelínek and Pokorný*, 1997] in the field of 300 A/m root-mean-square value. The sensitivity of the instrument, defined as the root-mean-square error in determining the magnetic susceptibility of a very weakly magnetic specimen, is 3×10^{-8} [SI]. This sensitivity enables the specimens with maximum minus minimum susceptibility difference equal to or larger than 3×10^{-7} to be reliably measured [*Hrouda*, 2002]. For example, the difference 3×10^{-7} corresponds to bulk magnetic susceptibility 3×10^{-5} and the degree of AMS (its definition is below) $P = 1.01$. As both the bulk susceptibility and the degree of AMS of the Land's End granite are larger (see below), the AMS determinations of the Land's End granite are reliable and can be interpreted accordingly.

[15] The data were statistically evaluated using the Anisoft 4.2. package of programs [*Jelínek*, 1978; *Hrouda et al.*, 1990; *Chadima and Jelínek*, 2008]. Two AMS parameters [*Jelínek*, 1981] were used to characterize the magnetic fabric defined by principal magnetic susceptibilities $k_1 \geq k_2 \geq k_3$. The intensity of the preferred orientation of magnetic minerals was indicated by the degree of anisotropy $P = k_1/k_3$. The character or symmetry of the magnetic fabric was defined by the shape factor $T = 2\ln(k_1/k_2) / \ln(k_2/k_3) - 1$, where $0 < T < 1$ constraints oblate and $-1 < T < 0$ prolate shapes of AMS ellipsoids. The orientation of the magnetic foliation and magnetic lineation is represented on lower hemisphere equal-area stereograms. In order to determine the contribution of particular minerals to the bulk rock magnetic susceptibility, we have analyzed bulk magnetic susceptibility variations with respect to temperature on powder specimens using the CS-3 Furnace and/or the CS-L Cryostat Apparatus and the KLY-3S Kappabridge [*Hrouda*, 1994; *Jelínek and Pokorný*, 1997].

4.1. Magnetic Mineralogy

[16] Contributions of particular minerals to the rock magnetic susceptibility and AMS were investigated through the method of maximum theoretical paramagnetic susceptibility (MTPS) and through magnetic susceptibility variation with temperature. The first method calculates the MTPS from the Fe and Mn contents determined by whole-rock geochemical analyses [e.g., *Aydin et al.*, 2007]. If the rock magnetic susceptibility is comparable to the MTPS, it is dominantly carried by paramagnetic minerals. In contrast, if the rock magnetic susceptibility is much higher than the MTPS, at least a part of Fe or Mn is likely to be contained in much more susceptible ferromagnetic minerals. The second method is based on characteristic features of magnetic susceptibility versus temperature curves such as Curie temperature and Verwey transition in ferromagnetics and hyperbola in paramagnetics. It was measured on coarsely powdered pilot specimens in temperature intervals of −194°C–0°C and 25°C–700°C, using the CS-L and CS-3 apparatuses [*Parma and Zapletal*, 1991], respectively, and KLY-3S or MFK1-FA Kappabridge. An approach developed by *Hrouda* [1994], based on the mathematical resolution of a part of the low temperature curve (usually between −180°C and −10°C) or of the initial part of the heating curve (usually between 25°C and 200°C) into a paramagnetic hyperbola and ferromagnetic straight line parallel to the abscissa, enables the contributions of paramagnetic and ferromagnetic fractions to the rock bulk magnetic susceptibility to be estimated.

[17] The mean bulk magnetic susceptibility (Km) of the Land's End granite is relatively low, ranging from 25×10^{-6} to 205×10^{-6} [SI] (Figure 4a). The Km values of the fine-grained granite are even lower ranging from 40×10^{-6} to 70×10^{-6}. The MTPS calculated from chemical analyses [*Chappell and Hine*, 2006; *Müller et al.*, 2006] corresponds well with the measured bulk magnetic susceptibility (compare Figures 4a and 4b). Consequently, it is highly likely that the predominant magnetic susceptibility carriers are paramagnetic minerals.

[18] The most conspicuous feature of the low temperature magnetic susceptibility variation is a relatively well-defined paramagnetic hyperbola without any indication of Verwey or Morin transitions (Figure 4c). In heating curves showing the high temperature magnetic susceptibility variation, the hyperbolas continue, though they are less conspicuous than in low temperature variation curves, again without any reliable indications of the Curie temperature (Figure 4d). The cooling curves show much higher susceptibilities indicating the creation of a new mineral similar to magnetite during heating (Figure 4d). The resolution of the magnetic susceptibility into paramagnetic and ferromagnetic components using the method described by *Hrouda* [1994] shows that at least 90% of the rock magnetic susceptibility is carried by a paramagnetic phase.

[19] As revealed microscopically, the possible paramagnetic phases within the Land's End granite are biotite and tourmaline. While biotite is relatively abundant and present in all specimens, tourmaline represents an accessory mineral phase (less than 1%) within the studied granite and is more localized in younger tourmaline granites and quartz-tourmaline veins [*Mintsa Mi Nguema et al.*, 2002; *Bouchez et al.*, 2006]. Consequently, we conclude that the susceptibility in our rocks is dominantly controlled by biotite.

[20] *Hrouda* [2010] showed that in rocks whose AMS is carried by two mineral fractions, one paramagnetic and one ferromagnetic, and where one fraction dominates the other one in bulk susceptibility, the rock AMS is relatively near to the AMS of the dominating fraction provided that the AMS of both fractions are comparable. This may not be true if the AMS of the dominating fraction is an order of magnitude lower than that of the other fraction. We have not found pyrrhotite and/or hematite whose grain AMS is an order of magnitude stronger than that of biotite. Magnetite, whose presence in very small amounts we cannot exclude, has AMS grain degree similar to that of biotite [cf. *Hrouda*, 1993]. Consequently, the AMS in our rocks is dominantly controlled by the lattice preferred orientation of biotite whose AMS is magnetocrystalline in origin.

4.2. Magnetic Fabric Characteristics

[21] The AMS data reveal a homogenous magnetic fabric throughout most of the Land's End granite (Figure 5). The magnetic foliation (perpendicular to K3) exhibits a variable orientation, but is commonly subhorizontal or gently dipping

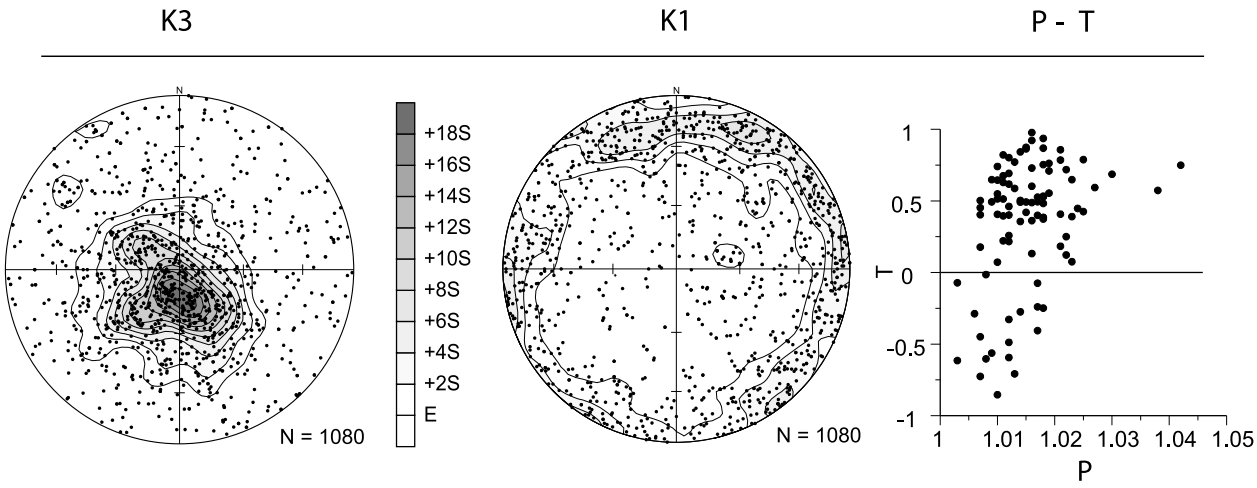

Figure 5. AMS data from the whole Land's End granite presented in stereographic projection show poles to magnetic foliations (K3) and lineations (K1) for 1080 samples. The P-T graph represents the shape and degree of AMS fabrics for each sample site.

to the NNW, SSE, or NE (Figure 5). The magnetic lineation [K1; *Henry*, 1997] shows weak preferred orientations in two main near-orthogonal directions, ENE–WSW and NNE–SSW to NNW–SSE. The AMS fabric exhibits a very low degree of anisotropy ranging from P = 1.005to P = 1.05, with several outliers; the mean value is P = 1.023 (Figure 5). These values are characteristic of a relatively weak biotite alignment that is usually observed in magmatic rocks lacking significant solid-state deformation [*Bouchez*, 2000]. The shapes of the AMS ellipsoid are dominantly oblate with few data points in the prolate field of the P-T plot (Figure 5).

5. Large K-feldspar Phenocryst Preferred Orientation Measured by Reflection Goniometry

5.1. Methodology

[22] The orientation of elongate triaxial K-feldspars defines a macroscopic planar magmatic fabric throughout most of the Land's End granite. However, it is difficult, if not impossible, to determine the magmatic lineation in the field. These difficulties are overcome through an optical reflection goniometry technique developed in order to precisely determine the orientation of large feldspar phenocrysts in oriented specimens [*Venera et al.*, 1996; *Schulmann et al.*, 1997]. This method allows the determination of not only the orientations of the magmatic foliation and lineation, but also the shape of feldspar fabric ellipsoid and the degree of preferred orientation.

[23] The biaxial optical reflection goniometer (Figure 6a) was used to measure the orientation of well-formed feldspar cleavages (Figure 6b). The position of the reflecting cleavage plane is defined by the two angles, an azimuth φ and an inclination τ (Figure 6a). The sample is fixed on the tracks so that the strike and dip of the oriented surface are parallel to the orthogonal tracks (dip = 0°). The fixed sample on the oriented surface is rotated around the vertical axis (up to 360°, azimuth φ) and simultaneously a collimator with a source of light beam rotates around the horizontal axis (inclination τ). The measurement is deducted when the light beam is exactly perpendicular to the measured plane.

[24] Feldspars have perfect (001) and good (010) cleavages. In this study, we have measured the (001) cleavage of the Carlsbad twins (Figure 6b). The angle between the pole to the (001) cleavage of each twin is approximately 50° and symmetrically clustered around the feldspar long axis; its orientation is then determined as the vector sum of the two pole orientations (Figure 6c). The foliation is perpendicular to the (010) plane and, in our case, is defined as a vector product of the two poles (Figure 6c). The resultant data are represented as mean lineation and foliation orientations, based upon a minimum of 30 twin measurements per specimen; these can then be compared to the corresponding AMS fabric elements. However, the AMS method provides other characteristics, derived from the magnetic susceptibility tensor, that allow the degree of anisotropy (P) and symmetry (T) of the AMS fabric to be described [*Jelínek*, 1981]. In order to characterize the fabric symmetry and intensity of the feldspar crystallographic preferred orientation (CPO), we have calculated a feldspar-shaped tensor in a similar manner as the AMS tensor. Every measured feldspar is characterized by three mutually orthogonal axes (1.2 : 0.6 : 0.2) oriented in space. The lengths of the axes, together with their orientations, define an ellipsoid. The sum of all the ellipsoid shapes and orientations measured in the sample is represented by a second order tensor that can be compared to the AMS tensor. The characteristics of the degree of feldspar CPO (P_f) and symmetry (T_f) are computed in a similar manner as the AMS parameters.

5.2. K-feldspar Fabric Characteristics

[25] The feldspars of the Land's End granite measured by reflection goniometry display long and short sectional ratios ranging from 1 to 21, with an average close to 5. In general, the measured fabric corresponds well to the observed field foliation, which supports the accuracy of our measurement. The goniometry was performed on several cross sections, which are indicated in Figure 1b. The detailed study sites are essentially located along coastal sections where outcrop quality is exceptionally high and allows three-dimensional (3D) structural analysis to be carried out; the poor exposure

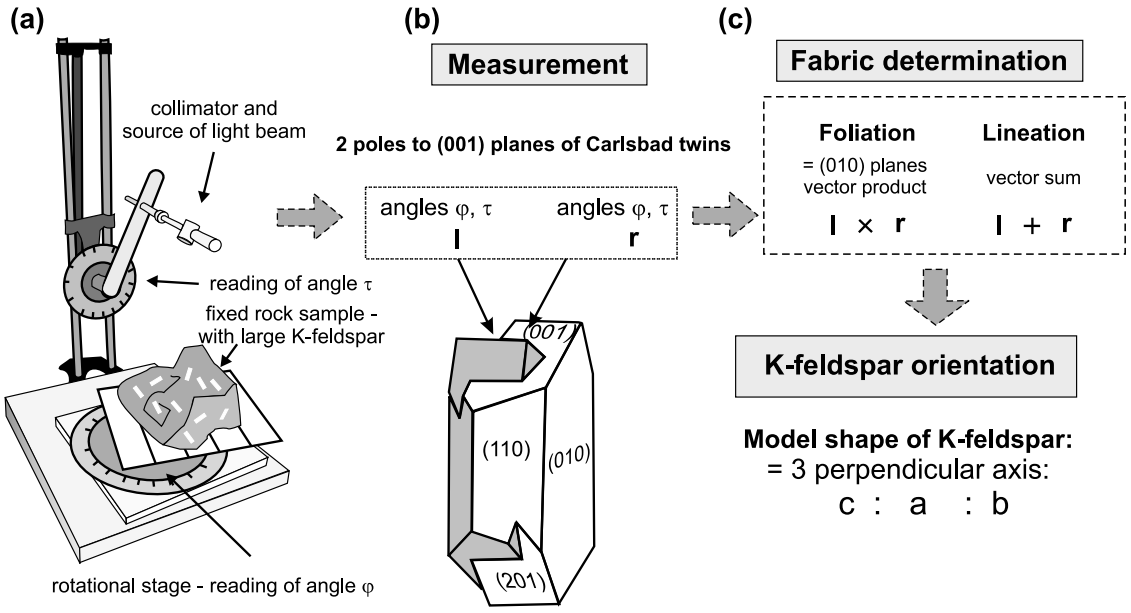

Figure 6. Scheme of the reflection goniometry method used to determine the large K-feldspar preferred orientation. (a) The reflection goniometer apparatus. (b) The measured declination and inclination angles define normal vectors (l and r) to two (001) planes of the Carlsbad twin. (c) The K-feldspar foliation is defined as a vector product of l and r and its lineation as a vector sum.

and degree of weathering in most inland parts of pluton precludes detailed fabric analysis. However, the coastal sections include sites both close to, and more remote from, the pluton boundaries and are considered to allow a reasonable insight into fabric development across the pluton at this exposure level.

[26] Fabrics measured by goniometry exhibit changes in orientation, symmetry, and intensity throughout the whole pluton. In general, the poles to (010) planes (b axes) show an extreme variability in orientation ranging from very steeply inclined to horizontal. However, when an eigenvalue analysis of the orientation tensor is applied, a weak maximum in the centre of the pole figure is obtained, indicating that a horizontal arrangement of the (010) plane statistically prevails (Figure 7). Similarly, the calculated feldspar c axes show high variability with a tendency to a girdle in the horizontal plane and a weak maximum located in the north. The parameters of P_f and T_f were plotted in the P_f-T_f diagram, in a similar manner as the AMS data. The feldspar fabric symmetry displays an extensive spectrum ranging from predominantly oblate ($T_f = 0.83$) to uncommon highly prolate fabrics ($T_f = -0.97$) (Figure 7). The degree of feldspar fabric intensity ranges from 1.3 to 3.1, with the average value $P_f = 2.2$. The interpretation of acquired P_f-T_f values is

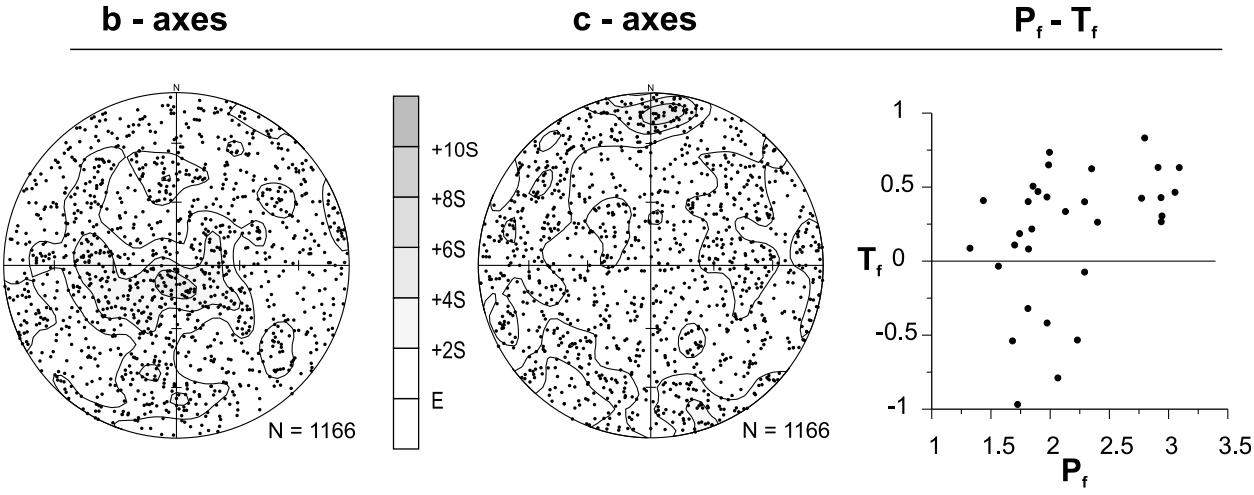

Figure 7. Results of the reflection goniometry presented in stereogram of poles to K-feldspar (010) planes = feldspar b axes and feldspar c axes for 1166 measurements. The P_f-T_f graph shows shape and degree of preferred orientation of feldspars for each sample site.

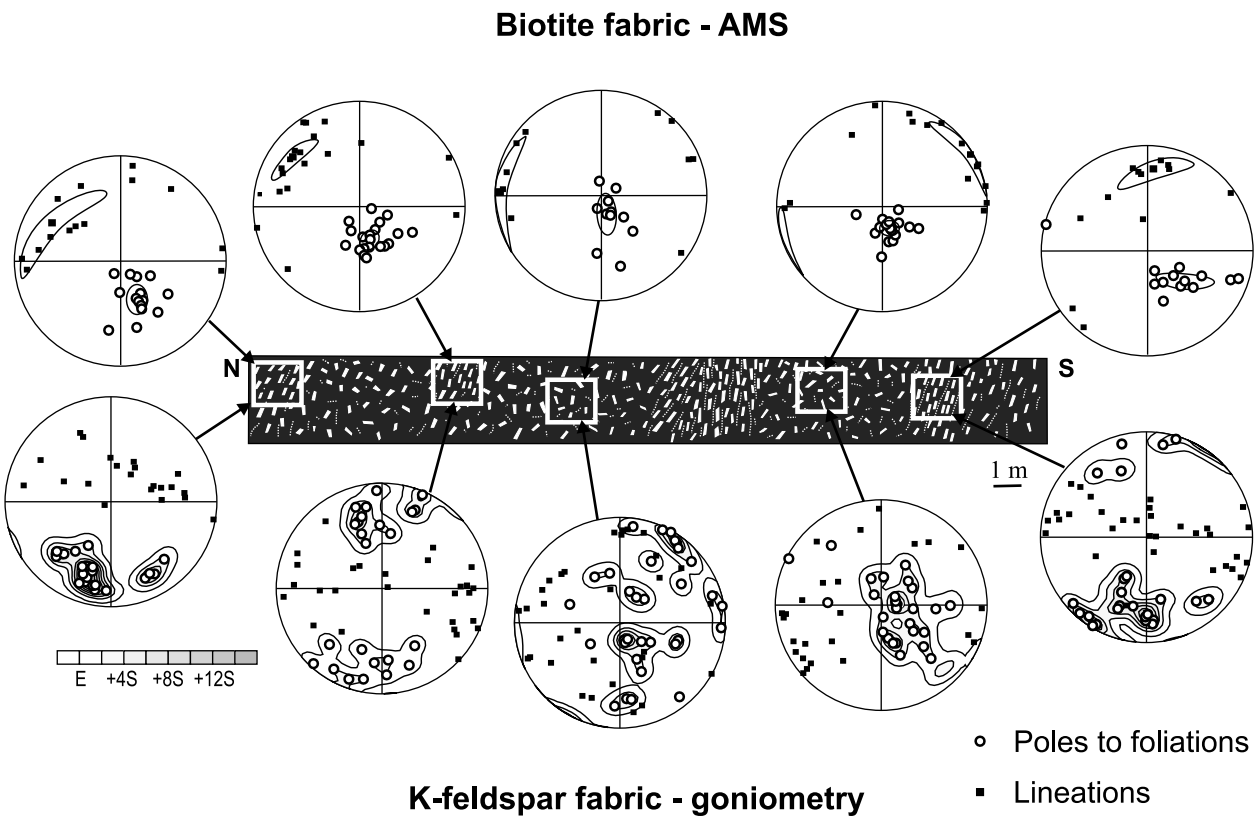

Figure 8. Schematic cross section illustrating the distribution of AMS and K-feldspar fabric patterns in relation to macroscopic variations of feldspar fabric intensities. Stereogram of poles to magnetic foliation (K3 direction) and lineations (K1 direction) for marked areas are presented in the upper row. Corresponding diagrams of K-feldspar b axes and c axes (emphasized with the contour lines) are shown in the lower row. Pole figures show data from one sample site.

not straightforward and will be discussed in the following section.

6. Correlation of K-feldspar and AMS Fabrics

[27] A potential problem with the quantitative comparison of the K-feldspar fabric with the biotite fabric is the different methods used for their determination. In the case of the K-feldspar fabric, the orientations of individual crystals were measured directly in terms of azimuth and plunge; in the case of the biotite fabric, the orientation was measured indirectly through AMS. In order to compare the K-feldspar fabric data and the biotite fabric data, two methods are used. The first calculates orientation tensors for both the directly measured K-feldspar data and the AMS (biotite) data. The second method constructs a shape tensor from the K-feldspar measurements that is formally the same as, and can be compared with, the AMS tensor.

[28] The preferred orientation of fabric elements in rocks is traditionally represented using contoured equal-area projections. Alternatively, the preferred orientation can be described mathematically by the orientation tensor [*Scheidegger*, 1965], where the principal values of the tensor (E1 > E2 > E3) are used to distinguish between cluster and girdle types of distribution. *Vollmer* [1990] introduced parameters derived from the principal values of the orientation tensor that enable the real distribution of the linear element under consideration to be replaced by a theoretical distribution [called equivalent distribution after *Jelínek et al.*, 1994] that is composed of three subdistributions: perfect cluster (C), perfect girdle (G), and the perfectly uniform (R). The respective parameters are defined as follows:

$$C = E_1 - E_2$$

$$G = 2(E_2 - E_3)$$

$$R = 3E_3.$$

It holds that $C + G + R = 1$.

[29] A straightforward relationship exists between the orientation tensor and the magnetic susceptibility tensor [for a summary, see *Ježek and Hrouda*, 2000]. For a rock, whose AMS is carried by a single magnetic mineral with an oblate rotational susceptibility ellipsoid like biotite [*Zapletal*, 1990; *Martin-Hernandez and Hirt*, 2003], the following relationship can be derived from the *Hrouda and Schulmann* [1990] and *Ježek and Hrouda* [2002] equations:

$$E_1 = (JP_c - 2LP_c - L)/J(P_c - 1)$$

$$E_2 = (JP_c - 2PP_c - P)/J(P_c - 1)$$

$$E_3 = (JP_c - 2PLP_c - PL)/J(P_c - 1)$$

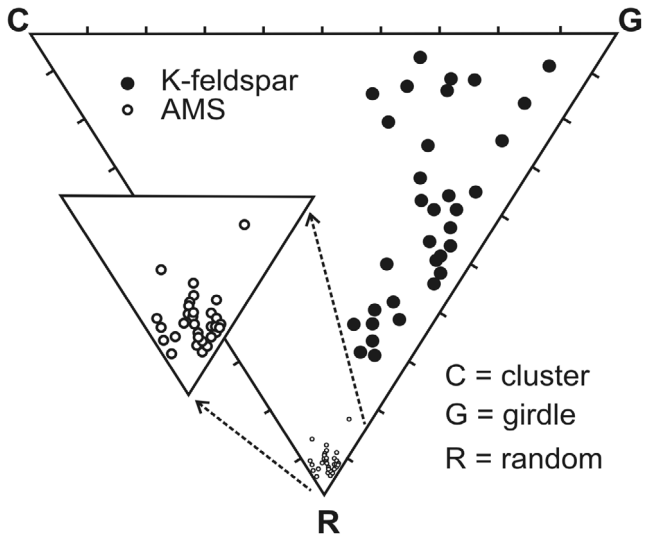

Figure 9. The triangular diagram plots the Vollmer`s three components [*Vollmer*, 1990; cluster, girdle, and uniform, the Vollmer`s random] computed from the eigenvalues. C characterizes the percentage of the fabric element have a perfect cluster orientation, G gives the percentage of fabric element with girdle orientation, and R is the parameter indicating the percentage of fabric element with the uniform distribution.

where $J = (PL + P + L)$, $P = k_1/k_3$, $L = k_1/k_2$, and P_c is degree of grain anisotropy (see Appendix).

[30] A comparison of the K-feldspar fabric with the biotite fabric should be made at the locality scale, because specimens for measuring K-feldspars and the AMS are different in size (cf. 1000 cm^3 versus 10 cm^3, respectively) and contain different numbers of grains (up to several tens of K-feldspar grains and about 1000 biotite grains). The mean AMS tensor for a locality was calculated using the Jelínek statistics [*Jelínek*, 1978] and the mean values obtained were used to determine the orientation tensor of normal to biotite (001) planes.

[31] We compare the K-feldspar and biotite fabrics in terms of their orientation and the intensity and shape of their fabric ellipsoids. Global fabric characteristics may be compared between AMS (Figure 5) and feldspar (Figure 7) indicating broadly similar patterns for the AMS and goniometry methods. Both planar fabrics show a horizontal maximum that is more pronounced by AMS, while the K-feldspar fabric exhibits considerably more variation. The similarity in fabric orientation, particularly AMS, over a large region suggests the existence of a common tectonic framework. It also implies that there might be a correlation between the AMS and K-feldspar fabrics on a local level. Nevertheless, examination of detailed data did not confirm this assumption.

[32] The local correlation and variability of the AMS and K-feldspar fabrics was evaluated in individual sample sites. There is no systematic change in fabric orientation with a location at the pluton scale, but there are at outcrop scale. These variations are demonstrated on a schematic cross section (Figure 8). It shows that changes in the intensity and orientation of the K-feldspar fabric creates domains of vertical NW–SE trending foliations (obliquely intersected) that are defined by an intense alignment of feldspars (compare Figure 2a) and domains with a rather chaotic fabric (Figure 2d). The accompanying stereograms summarize the AMS and feldspar fabric data from this same locality. The upper row of stereograms indicates similar subhorizontal AMS foliations along the whole profile. The lower row of stereograms indicates significant variations that correspond to the two different K-feldspar fabric intensities and orientations. The comparison of AMS and K-feldspar fabrics along this cross section demonstrates significant differences between the relatively stable subhorizontal AMS fabric and a variable feldspar fabric. It appears that the weak K-feldspar fabric is similar to the AMS fabric, while the intense K-feldspar fabric tends to be steeply inclined and occurs at high angles to the AMS fabric. This relationship is repeated in most of the cross sections studied across the Land's End granite.

[33] A detailed numerical evaluation of the AMS and K-feldspar fabric orientations at individual localities confirms the general differences shown in Figure 8. The AMS and K-feldspar foliations exhibit angular differences ranging from 0° to 90°. A statistical test of the colinearity between poles to the AMS and K-feldspar foliations [e.g., *Fisher et al.*, 1993, p. 225] rejects a correlation at 18 of 33 localities (on the 5% level). A similar result is obtained for the AMS and K-feldspar lineations (a correlation is rejected at 21 out of 33 localities). There are only seven localities where both the AMS and feldspar foliations and lineations do not possess statistically different orientations. Therefore, we conclude that there is no prevailing correlation between the AMS and feldspar fabric orientations at the local scale.

[34] The Vollmer plot (Figure 9) reveals that the biotite data for all localities investigated are concentrated near the R corner. This indicates a very weak preferred orientation of biotite. The K-feldspar values are much more scattered, being located at larger distances from the R corner and tending to create a wide line roughly parallel to the C-G line. Consequently, the K-feldspar fabric is remarkably stronger and different in symmetry.

[35] Because there is no systematic change in the orientation of the K-feldspar lineations and foliations with respect to geographical position, we have investigated whether the fabric data can be grouped or discriminated using other criteria, in particular the shapes and intensities of fabric ellipsoids. The most discriminating factor appears to be the intensity of the feldspar fabric (P_f). Figure 10 shows both AMS and K-feldspar fabrics split into three groups by different P_f-T_f values. The first row (Figure 10a, Type A fabric) shows the P_f values clustering around $P_f \sim 3$ indicating strongly oblate shapes. This feldspar fabric was observed together with a weak AMS fabric of variable, but mainly oblate shapes. The corresponding stereograms show that the intense K-feldspar fabric mainly comprises subvertical to steeply dipping foliations and steeply plunging lineations. In contrast, the AMS fabric comprises variable subhorizontal to moderately dipping foliations and predominantly gently plunging lineations. The second row (Figure 10b, Type B fabric) shows a feldspar fabric characterized by intermediate values clustering around $P_f \sim 2$. The foliation orientation is variable but has a weak sub-

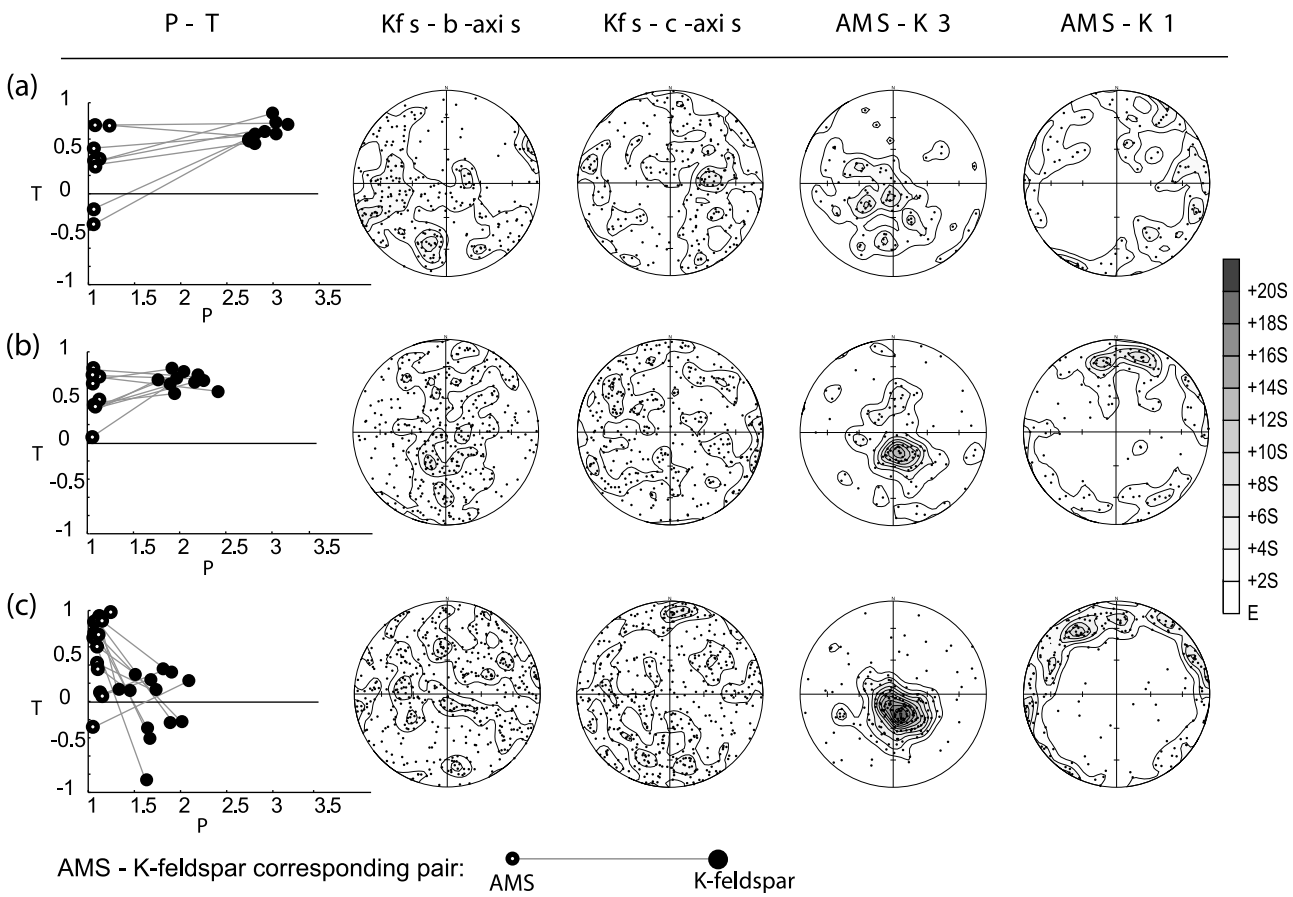

Figure 10. Discrimination of K-feldspar (Kfs) and AMS fabric data from the whole Land's End granite in three groups according to variations in P_f–T_f parameters of feldspar fabrics. (a) Type A subvertical strong (Pf ~ 3) and oblate feldspar fabrics are discordant to subhorizontal weakly aligned AMS fabrics. (b) Type B oblate, intermediate (Pf ~ 2) and subhorizontal K-feldspar fabrics are concordant with subhorizontal, dominantly oblate and well-aligned AMS fabrics. (c) Type C shows chaotic orientation distribution, weak (Pf ~ 1.6) and plane strain to prolate feldspar fabrics, and corresponding well-aligned subhorizontal and oblate AMS fabrics. In the P-T diagrams for K-feldspar (black circles) and AMS (open circles) fabrics from the same sample site are connected by tie lines.

horizontal maximum that is similar in orientation to the very strongly developed subhorizontal AMS foliation. AMS lineations are horizontal with a pronounced maximum toward N. The third row (Figure 10c, Type C fabric) shows a feldspar fabric characterized by a plane strain symmetry and lower fabric intensity (P_f ~ 1.6). The orientation of the K-feldspar foliation is highly variable and there is a weak subhorizontal N–S maximum to the lineation. This K-feldspar fabric again exhibits a significant deviation from the general AMS fabric that is characterized by a strongly defined subhorizontal foliation, gently NW and ESE plunging lineations, and a more strongly defined oblate AMS ellipsoid geometry.

[36] The grouping according to the intensity of the K-feldspar fabric (P_f) reveals important differences in terms of the individual fabric orientation distributions, symmetry, and intensity. The Type A and Type B fabrics correspond to two fabric groups described in the schematic cross section (Figure 8). Domains of concordance between the AMS and K-feldspar principal directions (Type B) are associated with the subhorizontal fabric patterns, an intermediate degree of K-feldspar preferred orientation, and a relatively uniform orientation of horizontal AMS fabrics. Domains of significant discordance between the AMS and feldspar fabrics (Type A) are related to steep, oblate, and intensive feldspar fabrics and horizontal, scattered AMS fabrics.

7. The Problem of Strong K-feldspar versus Weak AMS Fabrics

[37] In the previous paragraph we have defined three different groups of subfabrics on the basis of K-feldspar P_f values. This parameter was introduced as a formal analogue of the AMS tensor parameter P. The question is how to relate the P and P_f parameter. What values of P and P_f would represent the same deformation intensity if both K feldspars and biotites were reoriented by the same process and had the same deformation history? If all biotite grains were 100% aligned in one direction, their bulk magnetic susceptibility would have a P parameter equal to that of one grain (P ~ 1.3). For completely aligned feldspars, the corresponding P_f value would equal to the ratio of the longest to the shortest

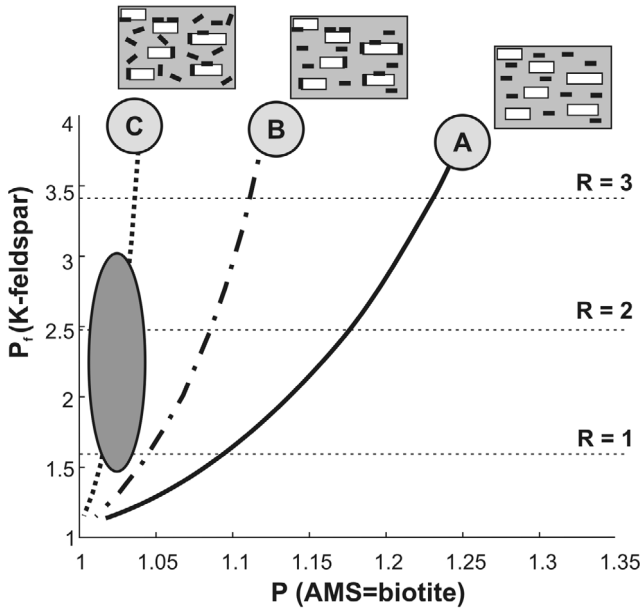

Figure 11. Numerical scaling of the K-feldspar fabric intensity expressed by parameter P_f. (a) Trajectory of the P_f (K-feldspar) and P (AMS = biotite) evolution in the pure shear (plane strain) type deformation. Horizontal lines show strain intensity R = log(X/Z). It is supposed that all biotites are free to rotate. (b) The model case for all biotites being attached to K-feldspars grain boundaries (100% of AMS is controlled by K feldspars). (c) 80% of biotites in the matrix are randomly oriented. AMS fabric is formed by 15% oriented biotites in the matrix and 5% attached to K-feldspar boundaries. The highlighted grey elliptic region shows the representative range of both K-feldspar and AMS data from the Land's End granite.

feldspar axes ($P_f \sim 6$). For a more detailed comparison, there is no simple relation or formula transforming the biotite P value to the corresponding feldspar P_f value. However, the scaling can be made numerically as follows. We consider a multigrain system composed of many biotites and K feldspars that are initially randomly oriented. The grains are then progressively reoriented by viscous flow and P and P_f values are computed for the same deformation increments. The results of calculations performed using the modified software of *Ježek and Hrouda* [2002] are shown in Figure 11. Line A shows the relationship between the P_f and P parameters as a function of incremental strain, e.g., for a K-feldspar fabric of intensity $P_f = 3$ (Type A fabric in Figure 10) the AMS fabric P value should be greater than 1.2 if the biotites and feldspars experienced the same deformation. However, the overall intensity of the biotite fabric measured in the Land's End granite is considerably lower, with typical P values between 1.01–1.04. This discrepancy in the biotite and K-feldspar fabric intensity requires a detailed examination of magmatic microstructure.

7.1. Textural Data and Numerical Assessment of the Biotite Fabric

[38] In order to characterize the individual fabric elements, we have conducted a detailed microstructural analysis and quantified the spatial distribution of minerals. The samples were cut parallel to the section defined by E1 and E3 eigenvectors of the feldspar orientation tensor, i.e., along the plane of the maximum preferred orientation of feldspar phenocrysts. The K-feldspar crystals were colored and the boundaries of minerals were manually traced and digitized from images in ArcView GIS. The phase objects were then statistically evaluated using the PolyLX Matlab toolbox [*Lexa*, 2003; *Lexa et al.*, 2005]. The quantification of the shape preferred orientation (SPO) of feldspars and biotite was expressed as the ratio of eigenvalues of the SPO tensor [*Lexa et al.*, 2005] and as rose diagrams with calculated mean preferred orientation and circular deviation.

[39] The Land's End granite displays a porphyritic texture with large euhedral K-feldspar phenocrysts surrounded by the mosaic of matrix minerals (mainly biotite, quartz, plagioclase, and K-feldspar, Figure 12). The large K-feldspar crystals occupy ~ 30% of the rock's volume and their shapes approximate triaxial polyhedra forming elongated and flattened tablets. Despite localized clustering of feldspar phenocrysts, the majority are isolated in a contiguous matrix (Figure 12). The biotite grains occur in two structural positions: attached to large euhedral feldspar phenocrysts or dispersed in the matrix. Some biotites may be attached along the feldspar crystal surfaces or even embodied within the large crystals along their growth zones (Figure 12). Matrix biotites occur in spaces between quartz and feldspar grains or form large aggregates composed of decussate biotite crystal intergrowths (Figure 12).

[40] The typical microstructural pattern is exemplified by two samples that demonstrate a contrasting relationship between the AMS and K-feldspar fabric. Sample n. 34a (Figure 13) is characterized by a vertical feldspar foliation and horizontal biotite foliation (Type A). The biotite reveals a lower aspect ratio (K = 1.75) compared to K feldspar (K = 2.40). The matrix biotite reveals a low and subhorizontal SPO that is oriented at a high angle to the weaker fabric defined by biotites attached to large feldspar crystals (Figure 13). The global SPO calculated for all biotites is weak (E1/E2 = 1.08) and has a preferred orientation subparallel to matrix subfabric. The SPO of feldspars is intense (E1/E2 = 2.14) and clearly oblique to that of matrix biotite. Sample n. 31 (Figure 14) is characterized by horizontal feldspar and AMS foliations (Type B fabric). In this sample, the biotites show low aspect ratios (K = 1.88) and very weak SPO (E1/E2 ranges between 1.08 and 1.10). In contrast, the K feldspars exhibit higher aspect ratio (K = 2.10) and significantly strong shape preferred orientation (E1/E2 = 1.81). In detail the biotite grains attached to large feldspars show a similar weak degree of SPO and similar orientation as the matrix biotites. The global fabric of biotite is therefore weak compared to strong K-feldspar fabric and reveals the same mean orientation.

[41] The quantitative microstructural analysis shows that there are two biotite subfabrics and they may make different relative contributions to the global biotite preferred orientation; this could explain the general weakness of global biotite fabric as reported by the AMS study. To test the relative contribution of the SPO of biotite grains attached to feldspar phenocrysts relative to the SPO of matrix biotites we have performed the following numerical simulations. We evaluate first the fabric of biotite attached to feldspars and compare it to that which would originate by passive rotation of originally randomly oriented biotite grains during viscous

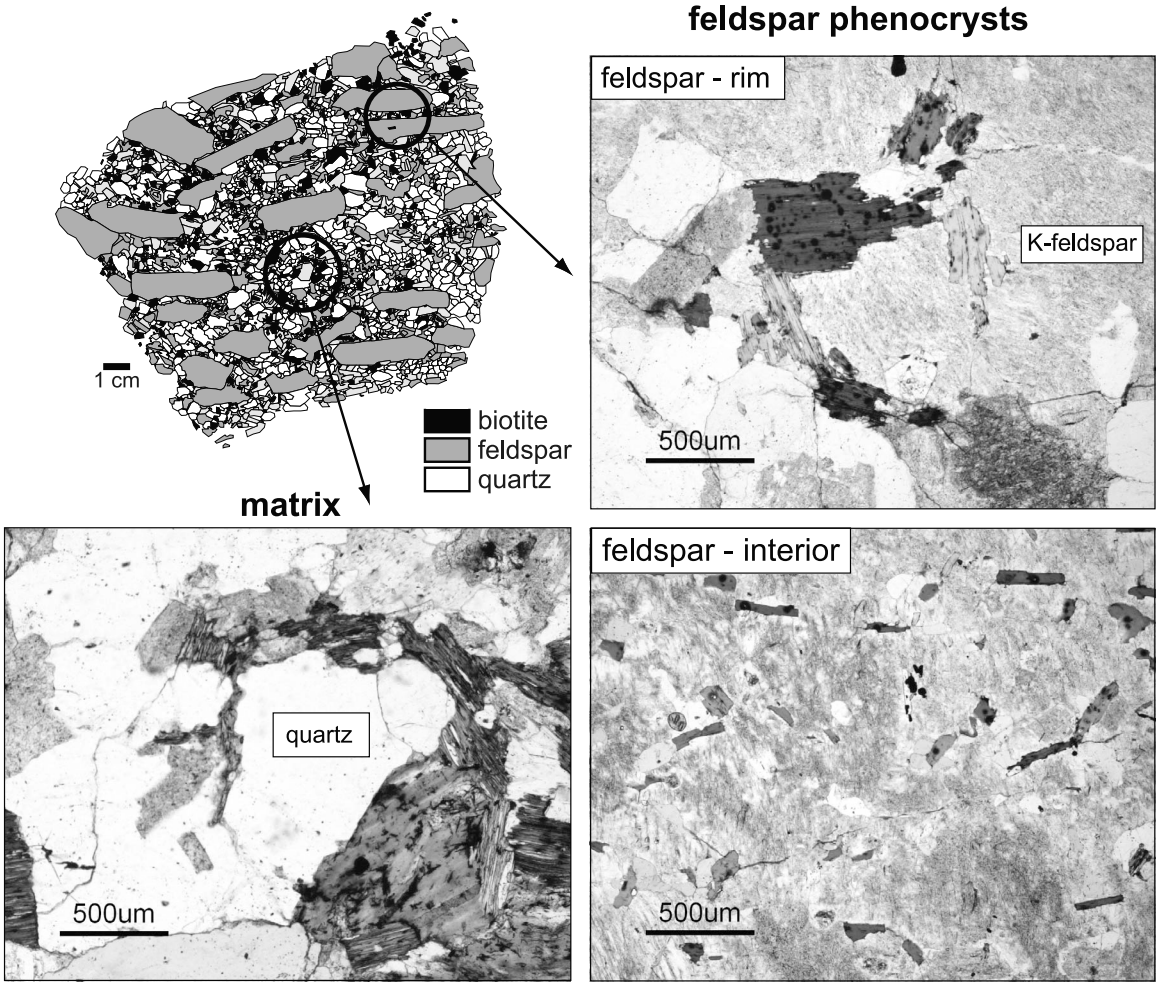

Figure 12. Details from the granite section. Photographs show biotites attached to the surfaces of large K feldspars and other matrix minerals and biotites aggregates randomly distributed within the matrix.

flow (Figure 11). Our model shows that the attached biotites create a magnetic subfabric that is different and probably less intense than fabric that would be created by matrix-hosted biotites in the same flow regime (path A in Figure 11). To estimate this effect, we carried out a numerical model of a feldspar crystal with biotites attached to all its surfaces. This combined microstructural element should behave mechanically as a feldspar but possess normalized principal magnetic susceptibilities of K1 = 1.052, K2 = 1.033, and K3 = 0.915 (P = 1.15, T = 0.75). If all biotite grains in the granite were attached to feldspars (or were in their zone of influence) in this manner, it would decrease the measured P value in the ratio 1.15 / 1.3 (i.e., by about 12%).

[42] Nevertheless, although this effect could decrease the biotite fabric intensity (P), the calculated values are still significantly greater than those measured in the Land's End granite, even if all biotite grains were attached to feldspars or their orientation was fully controlled by them. This is demonstrated in Figure 11, where path B corresponds to the model of 100% attached biotites. The P values decreased but are still too high compared to the AMS data. In addition, the analysis of oriented slabs (Figures 13 and 14) showed that biotite attached to feldspar represents only ~5–10% of the total biotite in the rock. Many of these are not perfectly aligned along feldspars and so attached biotites probably account for <10% of the fabric intensity. Therefore, the effect of biotites attached to feldspars does not adequately explain the difference in intensity of the K-feldspar and AMS fabrics. However, we note that despite the low proportion of biotites attached to K-feldspars, or located in their zone of influence, they may still play an important role in the measured AMS due to the intense orientation of K feldspars.

[43] The other contribution that should be assessed is that of biotite grains occurring in the matrix and representing about 85%– 95% of all biotite grains (Figures 12, 13, and 14). Here, the biotites are usually developed in the form of clusters or are macroscopically random (Figure 12). The microstructural analysis reveals that biotites are often attached to felsic matrix minerals, such as subhedral to anhedral plagioclase or quartz boundaries that are almost randomly oriented. Based on our microstructural analysis, only about 10%–15% of matrix biotites develop a preferred orientation and have a non-zero contribution to measured AMS, while the others are randomly distributed and oriented in the matrix.

[44] We finally evaluated the possibility that the AMS fabric is created by the combination of: (i) biotite attached to

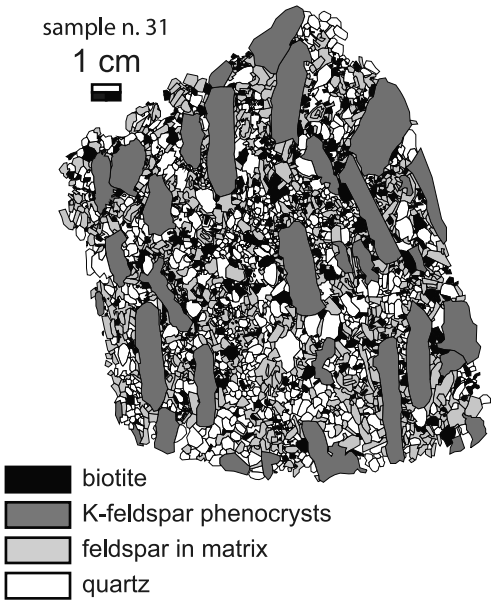

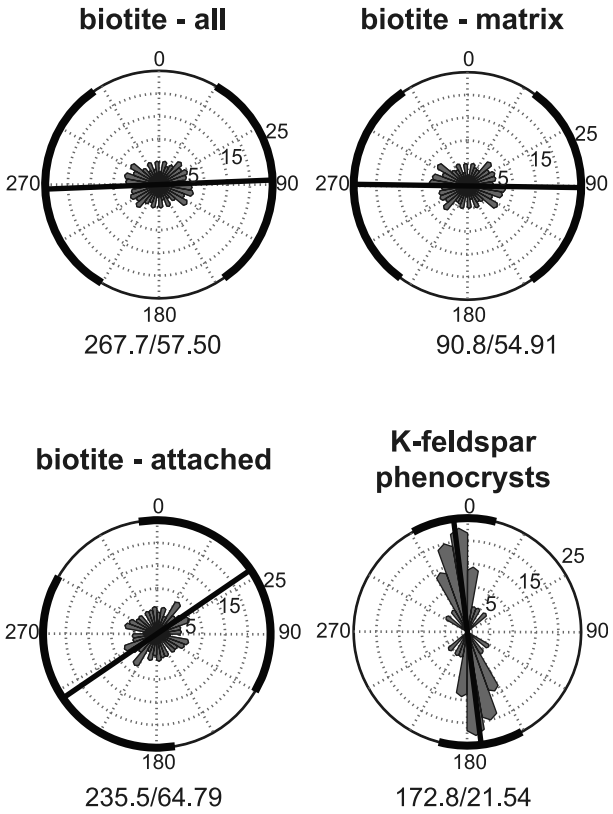

phase	E1/E2	K
biotite - all	1.08	1.75
biotitte - matrix	1.10	
biotitte - attached to Kfs	1.02	
K-feldspar - phenocrysts	2.14	2.39

Figure 13. Results of microstructural quantitative analysis of the sample with vertical K feldspars (n. 34a). The picture shows the digitized microstructure and calculated SPO using the PolyLX toolbox [*Lexa et al.*, 2005]. The SPO orientation is presented in form of frequency circular histograms (rose diagrams) and SPO intensity is given by the eigenvalue ratio of the SPO tensor (E1/E2). The values under each rose diagram correspond to SPO mean direction and standard circular deviation. The K number represents the mean axial ratio of minerals.

feldspar (5%), (ii) free and preferentially oriented biotite in the matrix (15%), and (iii) biotite in the matrix that is randomly oriented (80%). In Figure 11, path C shows that this scenario can satisfactorily account for the observed range of both P and P_f values. The microstructural study and modeling results concur and demonstrate that a weak matrix biotite preferred orientation may be weakened or strengthened by biotites attached to well-oriented feldspars depending on the angle between the feldspar and matrix biotite fabrics.

7.2. Differential Fabric Memory of Feldspar and Biotite

[45] Experimental petrology shows that biotite appears as one of the first minerals crystallizing from a granitic liquid [*Johannes and Holtz*, 1996]. Even if the biotite had the same deformation history as the feldspars, its early fabric would be extensively disrupted by the later crystallization of the felsic matrix minerals. Various processes may cause such fabric disintegration, but the most plausible is the attachment of small biotite grains to matrix feldspar boundaries during the late stages of matrix crystallization. The second possibility is that the orientation of the biotite grains was modified by interactions with similar sized matrix grains during late flow stages. These interactions generated deviations of biotite orientations in the flow field, thereby enabling further grain rotation and ultimate randomization of fabric. Indeed, *Tullis* [1977] has experimentally shown that the mutual interaction of biotite grains can significantly decrease fabric intensity and result in a deviation from predicted March behavior, which is supported by other experimental studies [*Ildefonse et al.*, 1992]. Whatever the mechanism of weakening the matrix biotite fabric, petrographic observations and quantitative assessment demonstrate that it is very weak, almost random, and largely controlled by matrix mineral boundary orientations (Figure 12).

[46] The origin of large K-feldspar crystals in granites still generates discussion between those who propose a magmatic origin as phenocrysts [*Vernon*, 1986; *Vernon and Paterson*, 2008] and those supporting a subsolidus origin, or modification, by metasomatism [*Stone and Austin*, 1961] or "textural coarsening" [*Higgins*, 1999; *Johnson et al.*, 2006]. In the Land's End granite, field observation, thin section analysis, and recently published mineral and whole rock geochemical data [*Müller et al.*, 2006] suggests magmatic growth. The occurrence of large K feldspars as inclusions within "xenoliths" in has also been cited as evidence for

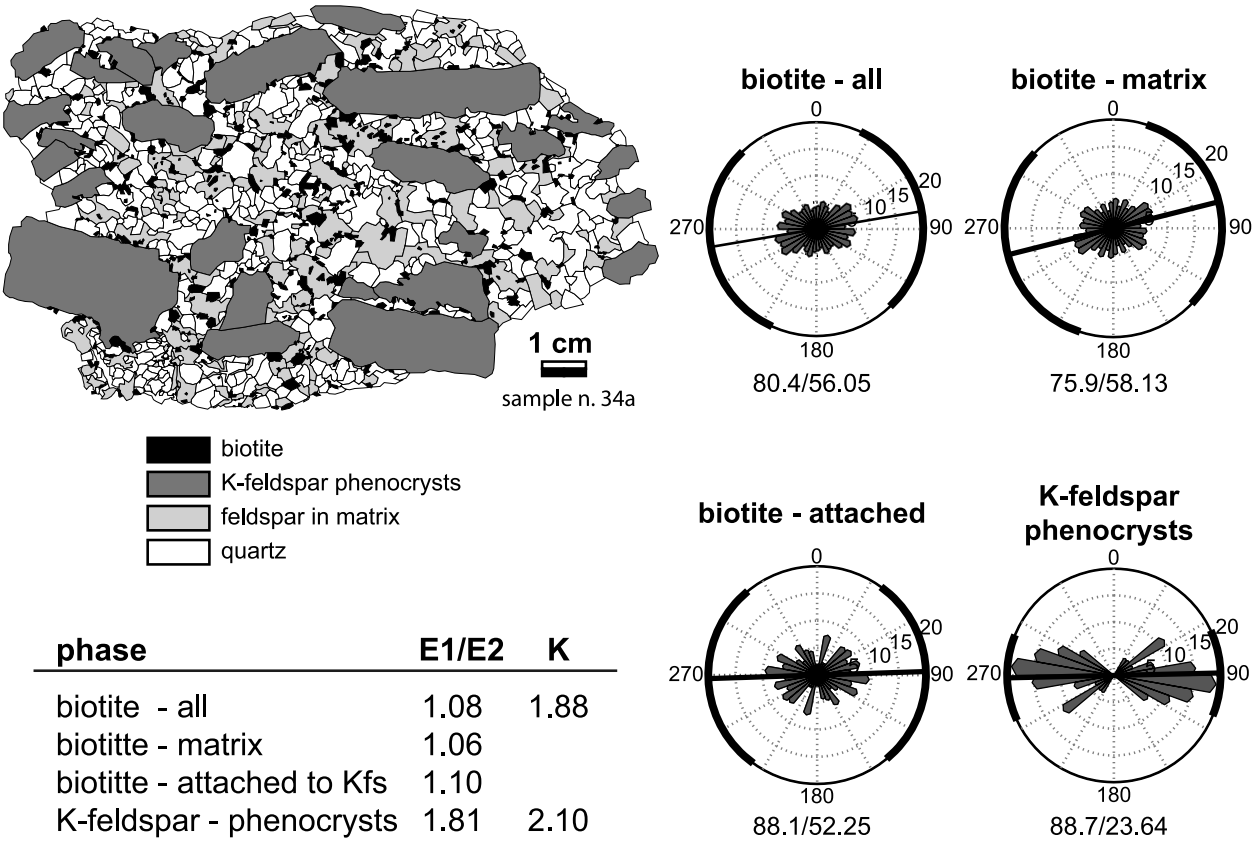

phase	E1/E2	K
biotite - all	1.08	1.88
biotitte - matrix	1.06	
biotitte - attached to Kfs	1.10	
K-feldspar - phenocrysts	1.81	2.10

Figure 14. Results of microstructural quantitative analysis of the sample with subhorizontal K feldspars (n. 31). The picture shows the digitized microstructure and calculated SPO using the PolyLX toolbox [*Lexa et al.*, 2005]. The SPO orientation is presented in form of frequency circular histograms (rose diagrams) and SPO intensity is given by the eigenvalue ratio of the SPO tensor (E1/E2). The values under each rose diagram correspond to SPO mean direction and standard circular deviation. The K number represents the mean axial ratio of minerals.

their metasomatic origin [*Stone and Austin*, 1961]. However, while these are common, they are restricted to microgranitoid enclaves and are absent from nonigneous enclaves [*Stimac et al.*, 1995]; they are consistent with an origin by magma mingling between host granite and hybridized microgranitoid magmas [e.g., *Vernon*, 1986; *Vernon and Paterson*, 2008]. Microstructural observations such as concentric zones of included biotite, quartz, and plagioclase in alkali feldspar [*Booth*, 1968] probably result from episodes of synneusis, possibly during periods of turbulent magma flow and mingling, followed by continued growth of the alkali feldspar in a magma, as supported by progressive core to rim changes in Rb, Sr, and Ba [*Müller et al.*, 2006]. The large phenocrysts therefore formed deeper in a magmatic system and were transported upward in the form of a crystal mush and noncrystallized residual melt. Variations in feldspar mineral chemistry suggest that the population at outcrop may be derived, through mingling, from different melt batches [*Müller et al.*, 2006].

[47] The feldspar crystals developed their fabric due to rigid body rotation during viscous flow of the surrounding magma in a manner that can be explained by the mathematical models of *Jeffrey* [1922] and *March* [1932]. According to these models the fabric intensity is a function of strain, i.e., the amount of magma displacement, while the shape of the fabric ellipsoid reflects the type of magmatic flow [*Ježek et al.*, 1994, 1996]. Consequently, the intense steep fabrics within the Land's End granite may reflect large magma displacements during the ascent and emplacement of the crystal-rich melt. These fabrics can only be modified by crystallization of the residual melt in the domain of magma emplacement and final cooling. We contend that the crystallization of matrix minerals cannot substantially alter the preferred orientation of large K-feldspar phenocrysts; these will retain their flow fabric with only minimal modification. However, this contrasts markedly with the small biotite crystals within the interstitial melt. As matrix feldspars and quartz grow, the intensity of the biotite fabric is progressively reduced. The K-feldspar phenocrysts therefore retain a much greater fabric "memory" than the matrix biotites. Moreover, a number of magma fabric studies show that the flow of magma can be highly partitioned, leading to the development of strong fabric variations related to a heterogeneous crystallization history during pluton assembly [e.g., *Schulmann et al.*, 1997; *Paterson and Miller*, 1998; *Vigneresse and Tikoff*, 1999]. We agree with these findings and suggest that variations in fabric intensity reported in this

work also reflect deformation partitioning during magma ascent.

8. A Model for Magmatic Fabrics: An Overprint on Complex Intrusive Fabrics

[48] The discrepancies between the biotite and K-feldspar fabrics in the Land's End granite are so large that they cannot result from a single deformation regime; they must reflect a complex kinematic history in combination with the different fabric memories of K feldspar and biotite. We propose that the fabric pattern originated by overprinting of ascent fabrics by late vertical shortening related to the pluton emplacement and possible regional tectonic deformation during pluton cooling. An analogous situation with contrasting feldspar versus AMS fabric patterns was observed by *Borradaile and Kehlenbeck* [1996] in granitoid plutons of the Canadian Shield. Here, the difference between the magnetic fabric preserved in the core of pluton and the strong circular alignment of feldspars along its margins was interpreted as a result of postmagmatic reactivation. Similarly, *Borradaile and Gauthier* [2003] studied an example of an Archean gneiss dome where the magnetic foliation formed a less convex domal surface than the field schistosity and was interpreted as a late inflation increment related to the diapiric rise of the gneiss dome. Although these results share several similar features with our study, we do not have constraints upon the fabric distribution across the whole of the Land's End pluton and therefore we cannot determine whether these are inflation-related fabrics associated with the diapiric rise.

[49] According to our data, we interpret the dominant intrusive fabric of the Land's End granite to be a vertical K-feldspar foliation. It is associated with a significantly weaker biotite fabric that was modified by matrix crystallization processes. Indeed, the correlation of field-based structural analysis with reflection goniometry measurements show that in regions with macroscopically measurable steep foliation, the goniometry provides the highest degree of feldspars preferred orientation (Figure 8). In contrast, in domains where the field measurements were impossible we have obtained weak feldspar preferred orientation. The degree of K-feldspar preferred orientation was therefore highly irregular across the whole granite body. This pattern is interpreted in terms of a highly partitioned granite emplacement, characterized by an alternation between domains of intensely and weakly developed vertical K-feldspar fabric end members. This complex intrusive fabric pattern was subsequently overprinted in the final emplacement phase by vertical shortening, during which the strong vertical K-feldspar fabric was weakened, but remained vertical, while the less intensive K-feldspar fabric was reoriented subhorizontally. The weak biotite fabric was homogeneously overprinted during this final deformation resulting in a subhorizontal AMS fabric throughout the whole Land's End granite. However, only a small percentage of biotites were effectively reoriented by the overprint and resulted in only a low intensity AMS; most biotites were randomized by the crystallization processes. Biotites attached on feldspar surfaces may also influence the final AMS.

[50] The vertical shortening, which produced the horizontal biotite fabric and some degree of reorientation of the K-feldspar fabric, may have been a consequence of: (i) modification of a subvertical magmatic flow, during the final stage of emplacement, by interaction with the roof of the contemporary magma chamber, formed by either the host rock or previous, now (largely) solidified, magma batches, (ii) post-emplacement magmatic-induced deformation related to the addition of later melt batches, or (iii) post-emplacement magmatic state regional deformation. It is not possible to resolve the relative contribution of each mechanism although (i) and (iii) are considered to be dominant. Fabrics generated by vertical shortening are often more intense within ~100 m or so of the host rock and the localized modification of magmatic fabrics along the northern margin of the Land's End granite, by interaction with host rock contacts and host rock xenoliths, has been described by *Kratinová et al.* [2003]. However, there is good evidence from mineralized fault systems, that vertical shortening, associated with regional NNW–SSE extension, persisted throughout the 20 Ma emplacement history of the Cornubian Batholith and was kinematically equivalent to the preemplacement ductile deformation of the host rock [*Shail and Wilkinson*, 1994; *Alexander and Shail*, 1995; *Shail and Alexander*, 1997]. AMS and fabrics in the Carnmenellis and Bodmin Moor granites have been interpreted to reflect postemplacement regional NNW–SSE extension [*Mintsa Mi Nguema et al.*, 2002; *Bouchez et al.*, 2006]. Although the Carnmenellis and Bodmin Moor granites are some 15–18 Ma older than the Land's End granite [*Chesley et al.*, 1993], we consider that the same regional deformation may have contributed to the late vertical shortening we have documented.

[51] In order to test this hypothesis, we constructed a numerical model of AMS and K-feldspar fabric development. Numerical modeling has been previously used to quantify the relationship between intensity and shape of the magnetic susceptibility ellipsoid [*Housen et al.*, 1993; *Benn*, 1994]. Recently, *Kratinová et al.*, [2007] and *Schulmann et al.*, [2009] examined, by means of numerical modeling, the effects of complex deformation overprints of magmatic fabrics in granites and partially molten rocks. These models provide an insight into variations in fabric symmetry and intensities that result from changes in the strength of the initial fabric and the orientation of deformation overprints. The results of our model are shown in Figure 15. We consider a multigrain system comprising biotite and K feldspar. K feldspars were initially oriented according to the two vertical intrusive fabric end members described above (Type A—strong and Type B—weak; Figure 10) and one case was chosen in between (Type C—medium). Biotite is considered to always define a weak initial vertical fabric. All grains are then reoriented by late emplacement plus tectonic strain and the corresponding biotite and K-feldspar fabrics computed. The grain reorientation is based on models of rigid body rotation in a viscous fluid [*Jeffrey*, 1922; *Willis*, 1977; *Ježek*, 1994]. Feldspars are considered as free to rotate due to their relative size with respect to the composition of matrix. Only 15% of biotites are considered free to rotate. We also consider 5% of biotites attached to feldspars parallel to their sides. The free and attached biotites create the AMS fabric.

[52] According to structural observations and available published data from the host rocks [*Shail and Alexander*, 1997], we assume that the late emplacement and tectonic deformation overprint corresponds to a combination of

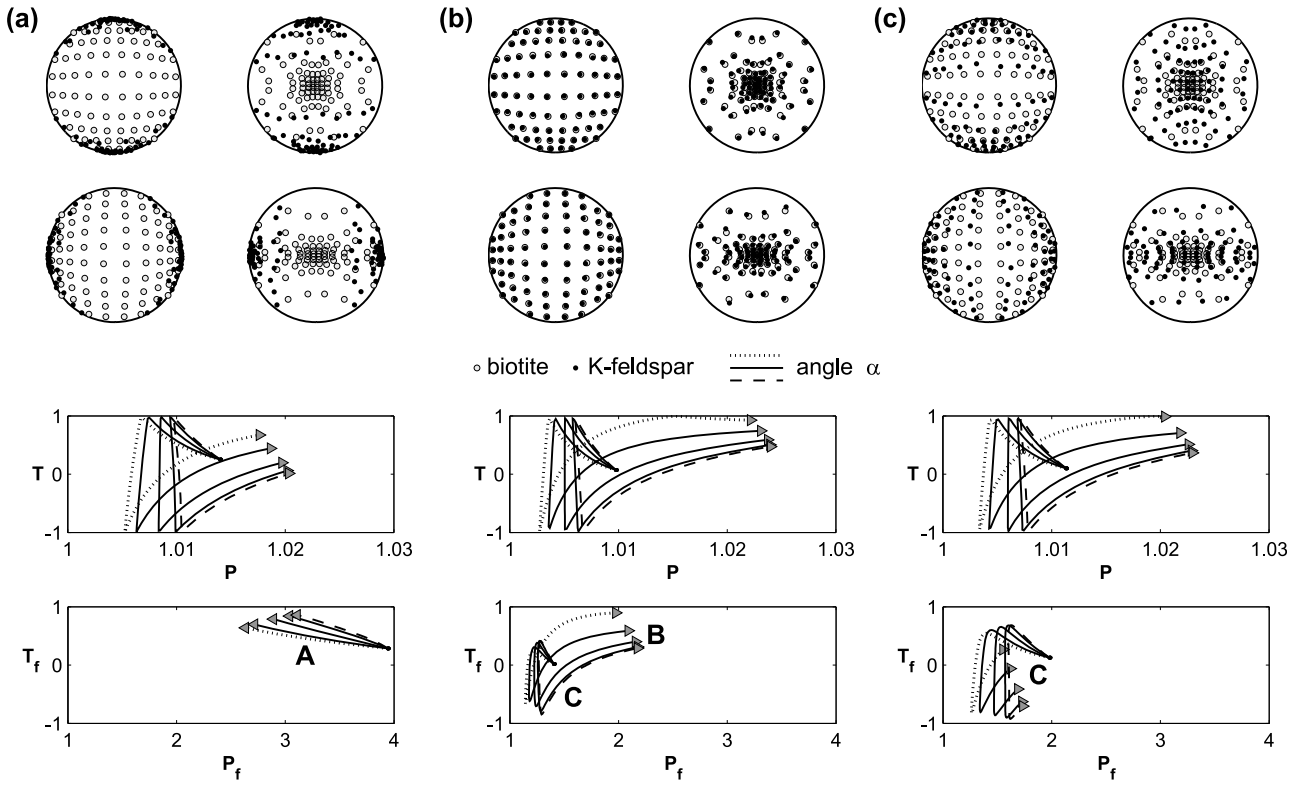

Figure 15. Numerical models representing simplified scenarios of fabric development for principal fabric types observed in the Land's End granite. Variable vertical pretectonic fabrics are subjected to a late deformation by vertical axial shortening and horizontal elongation. We consider five different mutual orientations ($\alpha = 0°, 22.5°, 45°, 67.5°, 90°$) of the emplacement and tectonic deformation. (a) Scenario of initially strong vertical K-feldspar fabric reworked to the observed A-type fabric. Pole figures present the initial (left) and final (right) distribution of poles to (010) planes of feldspars (black points) and (001) planes of biotite (symbol o). In the upper and lower row of pole figures the tectonic stretching component is perpendicular ($\alpha = 0$) and parallel ($\alpha = 90°$) to the vertical intrusive plane strain fabric, respectively (other α not shown). In the P-T (biotite, AMS) graph below, the former case ($\alpha = 0$) corresponds to the dotted P-T path and the latter ($\alpha = 90°$) to the dashed one. The cases of other α are shown by full lines. The P_f-T_f (K-feldspar) graph indicates the fabric type A described in text. (b) Scenario of initially low intensity K-feldspar vertical fabrics overprinted by the same deformation as in the previous case and resulting in the B-type fabric. C-type fabric may appear as a transient stage, not the fully developed B type. (c) Scenario of the C-type fabric developed due to late deformation (idem case a and b) superimposed on initially medium intensity K-feldspar fabric. In all cases, biotite fabric is formed by 15% of free biotites (with initially weak vertical orientation) plus 5% of biotites attached to K feldspars. The deformation overprint results in horizontal AMS fabric as it is observed in the whole Land's End granite.

vertical shortening (axial flattening) due to internal adjustment within the pluton driven by magma buoyancy and rigid lid effect of the granite roof, and plane strain deformation with vertical shortening and horizontal elongation associated with NNW–SSE regional extension. These two deformation components were applied simultaneously to an intrusive vertical plane strain fabric. Because the mutual orientation of emplacement-related and tectonic deformation may vary at different localities (in particular the angle α between the shortening axis of the intrusive plane strain and the stretching axis of the tectonic pure shear), we considered five different orientations ($\alpha = 0°, 22.5°, 45°, 67.5°, 90°$) for each run of the model.

[53] The first case (Figure 15a) starts with an initially strong vertical K-feldspar fabric. By progressive late emplacement and tectonic deformation (vertical shortening and plane strain) the K-feldspar fabric is weakened toward values about $P_f \sim 3$ but remains vertical. The AMS fabric is initially created by a low intensity vertical subfabric of 15% biotite in the matrix plus a subfabric of 5% biotite attached to K feldspar. During deformation, the weak fabric of the attached biotites is overprinted and starts to be replaced by a fabric developed from originally random biotites in the matrix, as they pass through a transient prolate toward oblate fabrics of degree $P \sim 1.02$. Five curves in the P-T graph, corresponding to different values of angle α, show the fabric variation that results from a variable orientation between the tectonic and intrusive deformation. The curves exhibit similar P values but different magnetic fabric shapes (ranging from oblate to prolate) and explain the natural

variation observed in our data. The K-feldspar fabric development corresponds to fabric type A shown in Figure 10.

[54] In the second case (Figure 15b), the initial K-feldspar fabric is vertical, but significantly weaker than in the previous case. During deformation, the matrix biotites create highly oblate fabrics, enhanced by the attached biotites. As the K-feldspar fabric intensity decreases, it switches to horizontal and its intensity increases again toward $P_f \sim 2$ creating a result that can be compared to the B-type fabric. The C-type fabric may form, as a transient stage, during the development of the B-type fabric.

[55] In the third case (Figure 15c), late deformation (idem case a and b) was superimposed on initially medium intensity K-feldspar fabric leading to C-type fabric.

[56] Given the number of parameters (intensity and orientation of assumed intrusive vertical fabric, the percentage of biotites attached to K feldspars, the proportion of biotites randomized by variable processes associated with matrix crystallization, and local variations of deformation overprinting the intrusive fabric) it is difficult to confirm in a more detailed way our hypothesis of the origin of observed fabrics. Nevertheless, we can conclude that in characteristic cases, the numerical model is in agreement with basic features observed in measured fabrics. This helps us to argue that the AMS and K-feldspar fabrics observed in the Land's End granite can be explained by our scenario of the partially decoupled strain memory of K feldspar and biotite and the complex late deformation overprint on intrusive magmatic fabrics.

9. Conclusions

[57] Our study revealed that the general agreement between AMS and feldspar fabrics at the scale of the whole Land's End pluton contrasts with important discrepancies in fabric intensity and mutual orientations of AMS and feldspar fabrics at outcrop scale. The AMS fabric is homogeneous and stable at a pluton scale, whereas the feldspar fabric reflects the strongly heterogeneous flow of crystal-rich magma comprising the record of partitioned flow and local fabric transposition.

[58] Detailed analysis of AMS, K-feldspar, and microstructural data indicate that each fabric reflects different parts of the magma cooling history and related fabric acquisition. We propose a model of fabric evolution in the Land's End granite whereby vertical feldspar fabrics of variable intensity were developed during initial emplacement. Subsequent vertical shortening, reflecting post-emplacement adjustment and regional tectonic deformation, is reflected primarily by the AMS fabric, while the feldspar fabric is only partially influenced.

[59] This study demonstrates the importance of matrix-scale and grain-scale crystallization processes that may significantly decrease biotite strain memory and result in low intensity AMS, due to the nonsystematic reorientation of a high percentage of biotite. This important effect has to be taken into account in applications of AMS if there is sufficient microstructural evidence. Similar considerations are required for biotites attached on other nonmagnetic but robust mineral grains reflecting the former tectonic history. Despite the low percentage of biotites with nonzero contribution to the measured AMS, the high sensitivity of the AMS method allows definition of the large-scale final tectonic overprint of the whole pluton.

[60] Modeling the simultaneous development of AMS and feldspar fabrics shows the importance of degree of feldspar fabric related to magma chamber material transfers and type of superposed deformation regime on the final fabric pattern. We propose that combined and quantitative study of nonmagnetic and magnetic fabrics can provide robust information about complex relationships between magma chamber construction and regional deformation.

Appendix A: Simplified Conversion of Magnetic Susceptibility into the Orientation Tensor

A1. Prolate Uniaxial Grains

[61] Consider a multigrain system composed of prolate uniaxial grains, each one with principal susceptibilities $K_1 > K_2 = K_3$, where $K_1 + K_2 + K_3 = 3$. The grains are identical in shape and magnetic properties and differ only by orientation. For such a system, *Ježek and Hrouda* [2002] found the equation

$$\mathbf{k} = \mathrm{K}\mathbf{I} + \Delta\mathbf{T} \tag{A1}$$

where k is bulk magnetic susceptibility, **T** is the orientation tensor of long grain axes, $K = K_2 = K_3$, $\Delta = K_1 - K_3$, and **I** is identity matrix.

[62] Eigenvectors of **k** and **T** are parallel. Therefore, without loss of generality, we can consider an equation containing only eigenvalues of both tensors

$$\begin{bmatrix} k_1 & 0 & 0 \\ 0 & k_2 & 0 \\ 0 & 0 & k_3 \end{bmatrix} = \begin{bmatrix} K_3 + (K_1 - K_3)E_1 & 0 & 0 \\ 0 & K_3 + (K_1 - K_3)E_2 & 0 \\ 0 & 0 & K_3 + (K_1 - K_3)E_3 \end{bmatrix} \tag{A2}$$

where $E_1 \geq E_2 = E_3$ are eigenvalues of the orientation tensor **T**, normalized as $E_1 + E_2 + E_3 = 1$. The eigenvalues of bulk magnetic susceptibility $k_1 \geq k_2 \geq k_3$ are normalized similarly as grain magnetic susceptibility, $k_1 + k_2 + k_3 = 3$.

[63] From equation (A2) the eigenvalues of the orientation tensor can be expressed as a function of the eigenvalues of bulk magnetic susceptibility and grain principal susceptibilities

$$E_1 = \frac{k_1 - K_3}{K_1 - K_3},\ E_2 = \frac{k_2 - K_3}{K_1 - K_3},\ E_3 = \frac{k_3 - K_3}{K_1 - K_3}$$

i.e.,

$$E_i = \frac{k_1 - K_3}{K_1 - K_3},\ i = 1, 2, 3 \tag{A3}$$

[64] In practice, uniaxial grains are conventionally represented by the degree of grain anisotropy $P_c = K_1/K_3$. Then

$$K_1 = \frac{3P_c}{2+P_c}, \quad K_3 = \frac{3}{2+P_c} \tag{A4}$$

and

$$E_i = \frac{\frac{k_i}{3}(2+P_c)-1}{P_c-1}, \quad i = 1,2,3 \tag{A5}$$

where, $k_1 + k_2 + k_3 = 3$.

[65] Instead of eigenvalues of bulk magnetic susceptibility, we sometimes use parameters $P = k_1/k_3$, $L = k_1/k_2$, $F = k_2/k_3$, $T = (2k_2 - k_1 - k_3) / (k_1 - k_3)$. Relevant formulas for the eigenvalues of the orientation tensor can be found by replacing k_i in the equation (A5) by one of the following options:

$$\begin{aligned}
&k_1 = \frac{3PL}{PL+P+L}, \; k_2 = \frac{3P}{PL+P+L}, \; k_3 = \frac{3L}{PL+P+L} \\
&k_1 = \frac{3P}{P+F+1}, \; k_2 = \frac{3F}{P+F+1}, \; k_3 = \frac{3}{P+F+1} \\
&k_1 = \frac{6P}{PT+3P-T+3}, \; k_2 = 3\frac{PT+P-T+1}{PT+3P-T+3}, \; k_3 = \frac{6}{PT+3P-T+3}
\end{aligned} \tag{A6}$$

[66] For example,

$$\begin{aligned}
E_1 &= \frac{\frac{PL}{PL+P+L}(2+P_c)-1}{P_c-1} \\
E_2 &= \frac{\frac{P}{PL+P+L}(2+P_c)-1}{P_c-1} \\
E_3 &= \frac{\frac{L}{PL+P+L}(2+P_c)-1}{P_c-1}
\end{aligned} \tag{A7}$$

or

$$\begin{aligned}
E_1 &= (2PL + PLP_c - J)/J(P_c-1) \\
E_2 &= (2P + PP_c - J)/J(P_c-1) \\
E_3 &= (2L + LP_c - J)/J(P_c-1)
\end{aligned} \tag{A8}$$

where $J = PL + P + L$.

A2. Oblate Uniaxial Grains

[67] If the multigrain system is composed of oblate uniaxial grains, previous equations change as follows. We consider principal grain susceptibilities $K_1 = K_2 > K_3$, where $K_1 + K_2 + K_3 = 3$. Equation (1) is valid but $K_1 = K_2 > K_3$, **T** is now the orientation tensor of short grain axes (poles to basal plane), $K = K_1 = K_2$, and $\Delta = -(K_1 - K_3)$. In equation (A2), the first and third eigenvalue of the orientation tensor interchange their positions

$$\begin{bmatrix} k_1 & 0 & 0 \\ 0 & k_2 & 0 \\ 0 & 0 & k_3 \end{bmatrix} = \begin{bmatrix} K_1-(K_1-K_3)E_3 & 0 & 0 \\ 0 & K_1-(K_1-K_3)E_2 & 0 \\ 0 & 0 & K_1-(K_1-K_3)E_1 \end{bmatrix} \tag{A9}$$

and

$$E_1 = \frac{K_1-k_3}{K_1-K_3}, \; E_2 = \frac{K_1-k_2}{K_1-K_3}, \; E_3 = \frac{K_1-k_1}{K_1-K_3} \tag{A10}$$

[68] Formulas (A4) and (A5) using degree of grain anisotropy P_c will change to

$$K_1 = \frac{3P_c}{2P_c+1}, \; K_3 = \frac{3}{2P_c+1} \tag{A11}$$

$$\begin{aligned}
E_1 &= \frac{P_c - \frac{k_3}{3}(2P_c+1)}{P_c-1}, \\
E_2 &= \frac{P_c - \frac{k_2}{3}(2P_c+1)}{P_c-1}, \\
E_3 &= \frac{P_c - \frac{k_1}{3}(2P_c+1)}{P_c-1}
\end{aligned} \tag{A12}$$

[69] Formulas containing the parameters P, L, F, and T can again be found by replacing k_i in equation (A12) from equation (A6). For example,

$$\begin{aligned}
E_1 &= \frac{P_c - \frac{L}{PL+P+L}(2P_c+1)}{P_c-1} \\
E_2 &= \frac{P_c - \frac{P}{PL+P+L}(2P_c+1)}{P_c-1} \\
E_3 &= \frac{P_c - \frac{PL}{PL+P+L}(2P_c+1)}{P_c-1}
\end{aligned} \tag{A13}$$

or

$$\begin{aligned}
E_1 &= (JP_c - 2LP_c - L)/J(P_c-1) \\
E_2 &= (JP_c - 2PP_c - P)/J(P_c-1) \\
E_3 &= (JP_c - 2PLP_c - PL)/J(P_c-1)
\end{aligned} \tag{A14}$$

where $J = PL + P + L$.

[70] **Acknowledgments.** This research was supported financially by the Czech National Foundation (GACR) (grant 205/03/0336), the Ministry of Education of the Czech Republic (project MSM0021620855, J. Ježek, O. Lexa, and F. Hrouda), the Grant Agency of the Academy of Sciences of the Czech Republic (GAAV) (grant KJB300120702 to Z. Kratinová), FCT project (AMS progress, PTDC/CTE-GIX/098696/2008 to Z. Kratinová), and grant of the French National Council (ANR "LFO in orogens" to K. Schulmann). We are grateful to Richard Scrivener for encouragement and help with field logistics, and to the British Geological Survey for financial support. The National Trust is thanked for permission to sample from their properties.

References

Alexander, A. C., and R. K. Shail (1995), Late Variscan structures on the coast between Perranporth and St.Ives, south Cornwall, *Proceedings of the Ussher Society*, *8*, 398–404.

Alexander, A. C., and R. K. Shail (1996), Late- to post-Variscan structures on the coast between Penzance and Pentewan, south Cornwall, *Proceedings of the Ussher Society*, *9*, 72–78.

Arthaud, F., and P. Matte (1977), Late-Palaeozoic strike-slip faulting in southern Europe and northern Africa: Result of a right lateral shear zone between the Appalachians and the Urals, *Bull. Geol. Soc. Am.*, *88*, 1305–1320.

Auréjac, J. B., G. Gleizes, H. Diot, and J. L. Bouchez (2004), The Quérigut Complex (Pyrennes, France) revised by the AMS technique: A syntectonic pluton of the Variscan dextral transpression, *Bull. Soc. Geol. Fr.*, *175*, 157–174.

Aydin, A., E. C. Ferré, and Z. Aslan (2007), The magnetic susceptibility of granitic rocks as a proxy for geochemical differentiation: Example from the Saruhan granitoids, NE Turkey, *Tectonophysics*, *44*, 85–95.

Benn, K., 1994. Overprinting of magnetic fabrics in granites by small strains: Numerical modeling, *Tectonophysics*, *233*, 153–162.

Booth, B. (1968), Petrogenetic significance of alkali feldspar megacrysts and their inclusions in Cornubian granites, *Nature*, *217*, 1036–1038, doi:10.1038/2171036a0.

Booth, B., and C. S. Exley (1987), Petrological features of the Land's End granites, *Proceedings of the Ussher Society*, *6*, 439–446.

Bouchez, J. L. (1997), Granite is never isotropic: An introduction to AMS studies of granitic rocks, in *Granite: from segregation of melt to emplacement fabrics*, edited by J. L. Bouchez, pp. 95–112, Kluwer Academic Publishers, Dordrecht.

Bouchez, J. L. (2000), Anistropie de susceptibilité magnétique et fabrique des granites, *C. R. Acad. Sci.*, *330*, 1–14.

Bouchez, J. L., T. Mintsa Mi Nguema, L. Esteban, R. Siqueira, and R. Scrivener (2006), The tourmaline-bearing granite pluton of Bodmin (Cornwall, UK): Magnetic fabric study and regional inference, *J. Geol. Soc. London*, *163*, 607–616.

Borradaile, G. J., and D. Gauthier (2003), Emplacement of an Archean gneiss dome, northern Ontario, Canada: Inflation inferred from magnetic fabrics, *Tectonics*, *22*(2), 1011, doi:10.1029/2002TC001443.

Borradaile, G. J., and B. Henry (1997), Tectonic applications of magnetic susceptibility and its anisotropy. *Earth-Sci Rev*, *42*, 49–93.

Borradaile, G. J., and M. Jackson (2004), Anisotropy of magnetic susceptibility (AMS): Magnetic petrofabrics of deformed rocks, In *Magnetic Fabric: Methods and Applications*, edited by F. Martin-Hernandez et al., Geological Society London, Special Publication, vol. 238, pp. 299–360.

Borradaile, G. J., and M. M. Kehlenbeck (1996), Possible Crypto tectonic magnetic fabrics in "Posttectonic" granitoid plutons of the Canadian Shield, *Earth and Planetary Science Letters*, *137*, 119–127.

Chadima, M., and V. Jelínek (2008), Anisoft 4.2. - Anisotropy data browser, 11th Castle Meeting, Bojnice, Slovakia, 22–28 June.

Chappell, B. J., and R. Hine (2006), The Cornubian Batholith: An example of magmatic fractionation on a crustal scale, *Resour. Geol.*, *56*, 203–244.

Chen, Y., A. H. Clark, E. Farrar, H. A. H. P. Wasteneys, M. J. Hodgson, and A. V. Bromley (1993), Diachronous and independent histories of plutonism and mineralization in the Cornubian Batholith, southwest England, *J. Geol. Soc. London*, *150*, 1183–1191.

Chesley, J. T., A. N. Halliday, L. W. Snee, K. Mezger, T. J. Shepherd, and R. C. Scrivener (1993), Thermochronology of the Cornubian batholith in southwest England: Implications for pluton emplacement and protracted hydrothermal mineralization, *Geochim. Cosmochim. Ac.*, *57*, 1817–1835.

Clark, A.H., Y. Chen, E. Farrar, and B. Northcote (1994), Refinement of the time/space relationships of intrusion and hydrothermal activity in the Cornubian batholith, Abstracts Volume, Ussher Society Annual Meeting, Minehead, January 1994.

Dangerfield, J., and J. R. Hawkes (1978), Variscan granites of South–west England, *Proceedings of the Ussher Society*, *4*(2), 158–171.

Dearman, W. R. (1971), A general view of the structure of Cornubia, *Proceedings of the Ussher Society*, *2*, 220–236.

Fisher, N. I., T. Lewis, and B. J. J. Embleton (1993), *Statistical analysis of spherical data*, 343 pp., Cambridge University Press, Cambridge, UK.

Flood, R. H., and R. H. Vernon (1988), Microstructural evidence of orders of crystallization in granitoid rocks, *Lithos*, *21*, 237–245.

Ghosh, P. K. (1934), The Carnmenellis granite: its petrology metamorphism and tectonics, *J. Geol. Soc. London*, 241–276.

Gleizes, G., G. Drevon, A. Asrat, and P. Barbey (2006), Structure, age and mode of emplacement of the Hercynian Borderes-Louron pluton (Central Pyrenees, France), *Int. J. Earth. Sci.*, *95*(6), 1039–1052.

Goode, A. J. J., and R. T. Taylor (1988), Geology of the country around Penzance, in *Memoir of the British Geological Survey*, Sheets 351 and 358 (England and Wales), 51 pp., HMSO, London.

Hawkes, J. R. (1981), A tectonic 'watershed' of fundamental consequence in the post-Westphalian evolution of Cornubia, *Proceedings of the Ussher Society*, *5*, 128–131.

Henry, B. (1997), The magnetic zone axis:a new element of magnetic fabric for the interpretation of the magnetic lineation, *Tectonophysics*, *271*, 325–329.

Higgins, M. D (1999), Origin of megacrysts in granitoids by textural coarsening: A crystal size distribution (CSD) study of microcline in the Cathedral Peak Granodiorite, Sierra Nevada, California, In *Understanding granites: integrating new and classical techniques*, edited by A. Castro et al., pp. 207–219, Geological Society of London Special Publication, vol. 168.

Housen, B. A., C. Richter, and B. A. van der Pluijm (1993), Composite magnetic anisotropy fabrics: Experiments, numerical models, and implications for the quantification of rock fabrics, *Tectonophysics*, *220*, 1–12.

Hrouda, F. (1993), Theoretical models of magnetic anisotropy to strain relationship revisited, *Phys. Earth Planet. Inter.*, *77*, 237–249.

Hrouda, F. (1994), A technique for the measurement of thermal-changes of magnetic-susceptibility of weakly magnetic rocks by the Cs-2 apparatus and Kly-2 kappabridge, *Geophys. J. Int.*, *118*(3), 604–612.

Hrouda, F. (2002), Low-field variation of magnetic susceptibility and its effect on the anisotropy of magnetic susceptibility of rocks, *Geophys. J. Int.*, *150*, 715–723.

Hrouda, F. (2010), Modelling relationship between bulk susceptibility and AMS in rocks consisting of two magnetic fractions represented by ferromagnetic and paramagnetic minerals—Implications for understanding magnetic fabrics in deformed rocks, *Journal of the Geological Society of India*, *75*(1), 254–266.

Hrouda, F., and J. Ježek (1999), Theoretical models for the relationship between magnetic anisotropy and strain: Effect of triaxial magnetic grains, *Tectonophysics*, *301*, 183–190.

Hrouda, F., and K. Schulmann (1990), Conversion of the magnetic-susceptibility tensor into the orientation tensor in some rocks, *Phys. Earth Planet. Inter.*, *63*(1–2), 71–77.

Hrouda, F., V. Jelínek, and L. Hrušková (1990), A package of programs for statistical evaluation of magnetic data using IBM-PC computers, *EOS Trans.*, AGU, San Francisco, pp.1289.

Hughes, S. P., R. J. Stickland, R. K. Shail, N. G. LeBoutillier, A. C. Alexander, and M. Thomas, (2009), The chronology and kinematics of late Palaeozoic deformation in the NW contact metamorphic aureole of the Land's End granite, *Geoscience in South–West England*, *12*, 140–152.

Ildefonse, B., D. Sokoutis, and N. S., Mancktelow (1992), Mechanical Interactions between Rigid Particles in a Deforming Ductile Matrix—Analog Experiments in Simple Shear-Flow, *J. Struct. Geol.*, *14*(10), 1253–1266.

Jeffrey, G. B. (1922), The motion of ellipsoidal particles immersed in a viscous fluid, *Proc. R. Soc. London*, *102*, 161–179.

Jelínek, V. (1978), Statistical processing of anisotropy of magnetic susceptibility measured on groups of specimens, *Studia geophysica et geodetica*, *22*, 50–62.

Jelínek, V. (1981), Characterization of the magnetic fabric of rocks, *Tectonophysics*, *79*, T63–T67.

Jelínek, V., and J. Pokorný (1997), Some new concepts in technology of transformer bridges for measuring susceptibility anisotropy of rocks, *Phys. Earth Planet. Inter.*, *22*, 179–181.

Jelínek, V., F. Hrouda, and D. H. Tarling (1994), New parameters for characterization of linear and planar elements using orientation tensor, in *Textures of geological materials*, edited by H. J. Bunge et al., pp. 393–399, DGM Verlag, Oberusel.

Ježek, J. (1994), Software for modeling the motion of rigid triaxial ellipsoidal particles in viscous flow, *Computers and Geosciences*, *20*(3), 409–424.

Ježek, J., and F. Hrouda (2000), The relationship between the Lisle orientation tensor and the susceptibility tensor, *Phys. Chem. Earth.*, *25*(5), 469–474.

Ježek, J., and F. Hrouda (2002), Software for modeling the magnetic anisotropy of strained rocks, *Computers and Geosciences*, *28*, 1061–1068.

Ježek, J., R. Melka, K. Schulmann, and Z. Venera (1994), The behaviour of rigid triaxial particles in viscous flows-modeling of fabric evolution in a multiparticle system, *Tectonophysics*, *229*, 165–180.

Ježek, J., K. Schulmann, and K. Segeth, (1996), Fabric evolution of rigid inclusions during mixed coaxial and simple shear flows, *Tectonophysics*, *257*, 203–221.

Johannes, W., and F. Holtz (1996), *Petrogenesis and Experimental Petrology of Granitic Rocks*, 335 pp., Springer-Verlag, Berlin Heidelberg.

Johnson, B. R., A. F. Glazner, and D. S. Coleman (2006), Potassium feldspar megacrysts in granites: Passive markers of magma dynamics or products of textural coarsening?, *EOS Transaction of the American Geophysical Union*, *87*(52), V51B–1670.

Kratinová, Z., K. Schulmann, F. Hrouda, and R. K. Shail (2003), The role of regional tectonics and magma flow coupling versus magmatic processes in generating contrasting magmatic fabrics within the Land's End granite, Cornwall, *Geoscience in south–west England*, *10*, 442–448.

Kratinová, Z., K. Schulmann, J. B. Edel, J. Ježek, and U. Schaltegger (2007), Model of successive granite sheet emplacement in transtensional setting: Integrated microstructural and anisotropy of magnetic susceptibility study, *Tectonics*, *26*, TC6003, doi:10.1029/2006TC002035.

Launeau, P., and A. R. Cruden (1998), Magmatic fabric acquisition mechanisms in syenite: Results of combined anisotropy of magnetic susceptibility and image analysis study, *J. Geophys. Res.*, *103*(B3), 5067–5089, doi:10.1029/97JB02670.

Launeau, P., and P.-Y. F. Robin (1996), Fabric analysis using the intercept method, *Tectonophysics*, *267*, 91–211.

Leveridge, B. E., M. T. Holder, and A. J. J. Goode (1990), Geology of the country around Falmouth, *Memoir for 1:50000 geological sheet 352 (England and Wales)*, British Geological Survey. HMSO, London.

Lexa, O. (2003), Numerical approaches in structural and microstructural analyses, PhD Thesis, Charles University, Prague.

Lexa, O., P. Štípská, and K. Schulmann (2005), Contrasting textural record of two distinct metamorphic events of similar P-T conditions and different durations, *J. Metamorph. Geol.*, *23*(8), 649–666.

March, A. (1932), Mathematische Theorie der Regelung nach der Korngestalt bei Affiner Deformation, *Z. Kristallogr.*, *81*, 285–298.

Martín-Hernández, F., and A. M. Hirt (2003), The anisotropy of magnetic susceptibility in biotite, muscovite and chlorite single crystals, *Tectonophysics*, *367*(1–2), 13–28.

Miller, R. B., and S. R. Paterson (1999), In defense of magmatic diapirs, *J. Struct. Geol.*, *21*, 1161–1173.

Miller, R. B., and S. R. Paterson (2001), Construction of mid-crustal sheeted plutons: Examples from the North Cascades, Washington, *Geol. Soc. Am. Bull.*, *113*(11), 1423–1442.

Mintsa Mi Nguema, T., R. I. F. Trindade, J. L. Bouchez, and P. Launeau (2002), Selective thermal enhancement of magnetic fabrics from the Carnmenellis granite (British Cornwall), *Phys. Chem. Earth*, *27*, 1281–1287.

Müller, A., R. Seltmann, C. Halls, W. Siebel, P. Dulski, T. Jeffries, J. Spratt, and A. Kronz (2006), The magmatic evolution of the Land's End pluton, Cornwall, and associated pre-enrichment of metals, *Ore Geol. Rev.*, *28*(3), 329–367.

Parma, J., and K. Zapletal (1991), CS-1 apparatus for measuring the temperature dependence of low-field susceptibility of minerals and rocks (in cooperation with KLT-2 Kappabridge), *Geofyzika Brno*, Unpublished Report.

Paterson, S. R., and R. B. Miller (1998), Stoped blocks in plutons: Paleoplumb bobs, viscometers, or chronometers?, *J. Struct. Geol.*, *20*(9/10), 1261–1272.

Paterson, S. R., R. H. Vernon, and O. T. Tobisch (1989), A review of criteria for identification of magmatic and tectonic foliations in granitoids, *J. Struct. Geol.*, *11*(3), 349–363.

Paterson, S. R., K. Fowler Jr., K. Schmidt, A. Yoshinobu, and S. Yuan (1998), Interpreting magmatic fabric patterns in plutons, *Lithos*, *44*, 53–82.

Rathore, J. S. (1980), A study of secondary fabrics in rocks from the lizard peninsula and adjacent areas in southwest cornwall, England, *Tectonophysics*, *68*, 147–160.

Rattey, P. R., and D. J. Sanderson (1984), The structure of SW Cornwall and its bearing on the emplacement of the Lizard Complex, *J. Geol. Soc. London*, *141*, 87–95.

Salmon, S. (1994), Mingling between coexisting granite magmas within the Land's End granite—preliminary observations, *Proceedings of the Ussher Society*, *8*, 219–223.

Scheidegger, A. E. (1965), On the statistics of the orientation of bedding planes, grain axes, and similar sedimentological data, *U.S. Geological Survey Professional Paper*, *525-C*, 164–167.

Schulmann, K., J-B. Edel, P. Hasalová, J. W. Cosgrove, J. Ježek, and O. Lexa, (2009), Influence of melt induced mechanical anisotropy on AMS fabrics and rheology of deforming migmatites, Central Vosges, France, *J. Struct. Geol.*, doi:10.1016/j.jsg.2009.07.004, *31*(10), 1223–1237.

Schulmann, K., J. Ježek, and Z. Venera (1997), Perpendicular linear fabrics in granite. Markers of combined simple shear and pure shear flow?, in *From segregation of melt to emplacement fabrics*, edited by J. L. Bouchez et al., pp.159–176, Kluwer Academic Publishers, Dordrecht.

Shail, R. K., and A. C. Alexander (1997), Late Carboniferous to Triassic reactivation of Variscan basement in the western English Channel: Evidence from onshore exposures in south Cornwall, *J. Geol. Soc. London*, *154*, 163–168.

Shail, R. K., and B. E. Leveridge (2009), The Rhenohercynian passive margin of SW England: Development, inversion and extensional reactivation, *CR ACAD SCI II A*, *341*, 140–155.

Shail, R. K., and J. J. Wilkinson, (1994), Late- to post-Variscan extensional tectonics in south Cornwall, *Proceedings of the Ussher Society*, *66*, 263–272.

Stimac, J. A., A. H. Clark, Y. Chen, and S. Garcia (1995), Enclaves and their bearing on the origin of the Cornubian batholith, southwest England, *Mineral Mag*, *59*, 273–296.

Stone, M., and W. G. C. Austin (1961), The Metasomatic origin of the Potash feldspar MegaCrysts in the granites of southwest England, *J Geol*, *69*(4), 464–472.

Tarling, D. H., and F. Hrouda (1993), *The Magnetic Anisotropy of Rocks*, 232 pp., Chapman and Hall, London.

Taylor, G. K. (2007), Pluton shapes in the Cornubian batholith: New perspectives from gravity modelling, *J. Geol. Soc. London*, *164*, 525–528.

Tullis, J., and R. A. Yund (1977), Experimental deformation of dry westerly granite, *J. Geophys. Res.*, *82*(36), 5705–5718, doi:10.1029/JB082i036p05705.

Venera, Z., K. Schulmann, R. Melka, and J. Ježek (1996), Fabric of porphyric magmatites inferred from the preferred orientation of feldspar phenocrysts, *Journal of Czech Geological Society*, *41*(3–4), 183–190.

Vernon, R. H. (1986), K-feldspar megacrysts in granites—Phenocrysts, not porphyroblasts, *Earth-Science Reviews*, *23*, 1–63.

Vernon, R. H., and S. R. Paterson (2008), How late are K-feldspar megacrysts in granites?, *Lithos*, *104*, 327–336.

Vigneresse, J. L., and B. Tikoff (1999), Strain partitioning during partial melting and crystallizing felsic magmas, *Tectonophysics*, *312*, 117–132.

Vollmer, F. W. (1990), An application of eigenvalue methods to structural domain analysis, *Geol. Soc. Am. Bull.*, *102*, 786–791.

Warr, L. N., T. J. Primmer, and D. Robinson (1991), Variscan very low-grade metamoirphism in southwest England: A distathermal and thrust-related origin, *J. Metamorph. Geol.*, *9*, 751–764.

Willis, D. G. (1977), A kinematic model of preferred orientation, *Geol. Soc. Am. Bull.*, *88*, 883–894.

Žák, J., K. Schulmann, and F. Hrouda (2005), Multiple magmatic fabrics in the Sázava pluton (Bohemian Massif, Czech Republic): A result of superposition of wrench-dominated regional transpression on final emplacement, *J. Struct. Geol.*, *27*(5), 805–822.

Žák, J., S. R. Paterson, and V. Memeti (2007), Four magmatic fabrics in the Tuolumne batholith, central Sierra Nevada, California (USA): Implications for interpreting fabrics patterns in plutons and evolution of magma chambers in the upper crust, *Geol. Soc. Am. Bull.*, *119*, 184–201.

Žák, J., K. Verner, and P. Týcová (2008), Multiple magmatic fabrics in plutons: An overlooked tool for exploring interactions between magmatic processes and regional deformation?, *Geol. Mag.*, *145*, 537–551, doi:10.1007/S0016756808004573.

Zapletal, K. (1990), Low-field susceptibility anisotropy of some biotite crystals, *Phys. Earth Planet. Inter.*, *63*, 85–97.

Ziegler, P. A., and P. Dèzes (2006), Crustal evolution of western and central Europe, in *European lithosphere dynamics*, edited by D.G. Gee and A.A. Stephenson, pp. 43–56, Geological Society of London Memoirs 32.

F. Hrouda, Agico Inc., Ječná 29a, CZ-621 00 Brno, Czech Republic.

J. Ježek, Institute of Applied Mathematics and Computer Sciences, Charles University, Faculty of Science, CZ-128 43 Prague 2, Czech Republic.

Z. Kratinová, Institute of Geophysics, Czech Academy of Sciences, Bočni II/1401, Prague, Czech Republic. (kratinova@ig.cas.cz)

O. Lexa, Institute of Petrology and Structural Geology, Charles University, Alberton 6, CZ-128, 43 Prague 2, Czech Republic.

K. Schulmann, Ecole et Observatoire des Sciences de la Terre, Institut de Physique du Globe - CNRS UMR 7516, Université de Strasbourg, 1 rue Blessig, F-67084, Strasbourg CEDEX, France.

R. K. Shail, Camborne School of Mines, College of Engineering, Mathematics and Physical Sciences, University of Exeter, Cornwall Campus, Penryn, TRIO 9EL, United Kingdom.